TU Delft

Delft University of Technology

Local re-immersion behaviour of Ce-based inhibiting layers on AA2024-T3 intermetallics: Enhanced stability through partial dealloying and prolonged exposure

Mopon, Marlon; Mol, Arjan; Garcia, Santiago J.

DOI
10.1016/j.corsci.2025.113146

Publication date
2025

Document Version
Final published version

Published in
Corrosion Science

Citation (APA)
Mopon, M., Mol, A., & Garcia, S. J. (2025). Local re-immersion behaviour of Ce-based inhibiting layers on AA2024-T3 intermetallics: Enhanced stability through partial dealloying and prolonged exposure. *Corrosion Science*, *255*, Article 113146. https://doi.org/10.1016/j.corsci.2025.113146

Important note
To cite this publication, please use the final published version (if applicable).
Please check the document version above.

Copyright
Other than for strictly personal use, it is not permitted to download, forward or distribute the text or part of it, without the consent of the author(s) and/or copyright holder(s), unless the work is under an open content license such as Creative Commons.

Takedown policy
Please contact us and provide details if you believe this document breaches copyrights.
We will remove access to the work immediately and investigate your claim.

This work is downloaded from Delft University of Technology.
For technical reasons the number of authors shown on this cover page is limited to a maximum of 10.

Corrosion Science 255 (2025) 113146

Contents lists available at ScienceDirect

Corrosion Science

journal homepage: www.elsevier.com/locate/corsci

Local re-immersion behaviour of Ce-based inhibiting layers on AA2024-T3 intermetallics: Enhanced stability through partial dealloying and prolonged exposure

Marlon Mopon Jr. [a,b,*], Arjan Mol [c], Santiago J. Garcia [a,**]

[a] Aerospace Structures and Materials Department, Delft University of Technology, Delft, the Netherlands
[b] Department of Chemical Engineering, University of the Philippines Diliman, Quezon City, Philippines
[c] Department of Materials Science and Engineering, Delft University of Technology, Delft, the Netherlands

ARTICLE INFO

Keywords:
Re-immersion stability
Inhibition stability
Local corrosion
In situ microscopy
AA2024

ABSTRACT

The stability of inhibiting layers on AA2024-T3 intermetallic particles (IMPs) during re-immersion in saline following an initial immersion in a Ce(III)-containing electrolyte was investigated using in situ reflected light microscopy. Re-immersion behaviour varied due to differences in IMP composition, spatial distribution, and Ce (III) precipitation. IMPs were grouped into four categories based on whether their activity was high or low during both the immersion and re-immersion stages. Majority of the high activity particles during re-immersion had low activity during immersion. Longer immersion times (up to 72 h) and a brief delay in inhibitor supply (30 s) reduced re-immersion activity by increasing Ce(III) coverage. These findings suggest that corrosion protection systems promoting greater Ce(III) precipitation may enhance re-immersion stability.

1. Introduction

AA2024-T3 is broadly used in the aerospace industry due to its excellent strength-to-weight ratio. However, intermetallic particles (IMPs) formed during thermomechanical processing make the alloy prone to localized corrosion when exposed to harsh environments [1–3]. To address this, coatings are applied to shield the metal from corrosive agents. Additionally, incorporating corrosion inhibitors into the coatings [4–8] provides active protection, complementing their passive barrier function. This active protection becomes particularly valuable when the coating sustains mechanical damage, exposing the underlying metal. The damaged coating releases inhibitors which interact with the exposed metal surface to slow or prevent further corrosion. The recommended release rate is dependent on the environment and corrosion inhibitor. Oltra et al. [9] showed that there is a competition between inhibitor mass transport and the triggering time of local corrosion. This competition leads to preference for systems with initial fast release to minimize local corrosion on the exposed metal surface [10,11].

Corrosion inhibitors released from active protection systems mainly target the surface of IMPs in AA2024-T3, although they can also affect the bulk matrix [12,13]. However, it's the interaction with the IMP surface that plays the most important role in preventing local corrosion. The specific nature of this interaction is determined by the chemistry of the inhibitor, the surface state, and the environmental conditions. For example, rare earth metal inhibitors such as $Ce(NO_3)_3$ mainly form local inhibiting layers through precipitation, as the cation reacts with hydroxide ions generated during the dealloying of IMPs [14–16]. Organic inhibitors like 2,5-dimercapto-1,3,4-thiadiazole (DMTD), on the other hand, form inhibiting layers by adsorbing on the particle surface [13,17]. Regardless of the inhibitor chemistry, long-term effectiveness of protection depends on a consistent inhibitor supply as this can limit potential stability loss of the inhibiting layer [10,11,18]. This has translated to active corrosion protection design strategies that give preference to prolonged or sustained inhibitor release [19,20]. However, when inhibitors are embedded within coatings, their finite storage capacity limits long-term inhibitor availability. Inevitable depletion of the inhibitors in the coating can thus cut off inhibitor supply and leave damage sites vulnerable to failure of inhibition and corrosion attack.

Ensuring stable inhibition even when the inhibitor supply is cut off is essential for reliable active protection of AA2024-T3. However, the mechanisms of inhibition failure in a post-cut off scenario remain underexplored, as corrosion inhibitor performance is mostly evaluated

* Corresponding author at: Aerospace Structures and Materials Department, Delft University of Technology, Delft, the Netherlands.
** Corresponding author.
E-mail addresses: m.mopon@tudelft.nl (M. Mopon), s.j.garciaespallargas@tudelft.nl (S.J. Garcia).

https://doi.org/10.1016/j.corsci.2025.113146
Received 5 April 2025; Received in revised form 11 June 2025; Accepted 24 June 2025
Available online 25 June 2025
0010-938X/© 2025 The Authors. Published by Elsevier Ltd. This is an open access article under the CC BY license (http://creativecommons.org/licenses/by/4.0/).

in environments with continuous inhibitor availability [21–24]. Homborg et al. simulated inhibitor-depleted conditions by re-immersing AA2024-T3 in an inhibitor-free corrosive environment (e.g., 0.05 M NaCl) after initial exposure to inhibitors like $Ce(NO_3)_3$ and phytic acid [25]. Their in situ optical-electrochemical analysis revealed that Ce $(NO_3)_3$ provides relatively stable corrosion protection but is still prone to localized failure at IMPs. Similarly, Zhao et al. found that small NaCl concentrations (0.025 – 0.25 M) can lead to higher degree of DMTD chemisorption during immersion, making it more stable during re-immersion in saline environments without inhibitors [13]. They also showed that loss of inhibition, when present, is also initially observed on the surface of IMPs.

Visser et al. also explored inhibition stability during re-immersion and demonstrated that Li_2CO_3 has greater stability compared to 2-MBT and BTA [26]. They attributed the lower re-immersion stability of 2-MBT and BTA to the desorption tendency of the inhibiting layer previously formed. Li et al. deepened in the topic and showed the irreversibility of Li_2CO_3 conversion layers using electrochemical noise analysis and highlighted their vulnerability to localized damage under certain exposure conditions [27]. While these studies offer useful information about how different inhibitors perform during re-immersion, we still lack a clear understanding of how inhibition failure starts and spreads at the local level. Closing this gap is important for improving the reliability of active corrosion protection strategies for AA2024-T3.

This work investigates the stability, and/or loss of stability, of inhibiting layers formed on IMPs in AA2024-T3 during re-immersion in a corrosive environment. This study primarily examines how IMPs respond in inhibitor-free conditions, with their initial behaviour in the presence of inhibitors considered for context. By analysing the re-immersion behaviour, this study helps identify the factors that could lead to inhibition failure and contributes to the development of more durable corrosion protection strategies. This builds on our previous work [28] which examined how variations in inhibitor introduction at the start of exposure influenced inhibition performance under continuous inhibitor presence. In contrast, the present study shifts the focus to the other end of the inhibition timeline - when the inhibitor is no longer present in the system. Using in situ reflected light microscopy (RM), we monitored the behaviour of a large number of IMPs with high spatial and temporal resolution to assess how inhibition changes over time in the absence of continued inhibitor availability. High spatial resolution enables detailed analysis at the level of individual IMPs, while high temporal resolution is essential for capturing the rapid and dynamic processes involved in corrosion initiation. Notably, other local techniques are capable of providing more quantitative information about local corrosion development and inhibition failure on IMP sites. For example, scanning vibrating electrode technique can be used to analyse local ionic current densities to determine where local cathodic and anodic sites develop [29–32]. Scanning ion-selective electrode technique can be used to analyse local pH changes which can give insight about the progression of local corrosion [30–33]. Kelvin probe techniques (e.g., scanning Kelvin probe, scanning kelvin probe force microscopy) can be used to measure local work functions which can be used as indicators of local corrosion resistance [30–32,34]. Despite the local quantitative information that can be obtained from these techniques, they usually need to trade wide sampling area for good temporal and/or spatial resolution [30–32]. In situ RM is less sensitive to this limitation which makes it useful for tracking time-dependent surface changes over multiple sites simultaneously. The technique was thus used to monitor local surface changes arising from the formation of the inhibiting layer during immersion and monitor how these layers evolved during re-immersion. Analysing inhibition and its breakdown across many sites is essential for developing a more complete understanding of inhibitor performance. This broader approach allows us to identify the full range of re-immersion behaviour and which types of local failure are most critical to the stability of corrosion protection. Such insights are especially important for AA2024-T3, where even a single point of failure can compromise macroscale performance. $Ce(NO_3)_3$, referred to as Ce (III), served as the model inhibitor for this study.

We also looked at how the duration of exposure to inhibitor solutions and the delay in supplying the inhibitor affect the stability of the inhibiting layers during re-immersion. These two factors mimic common design strategies used in active corrosion protection coatings: exposure time is related to sustained release, while supply delay relates to initial release rates. In the fast initial release scenario, the inhibitor is present from the start of immersion (undelayed supply). Meanwhile in the slow initial release scenario (delayed supply), the metal is first exposed to a corrosive environment for a set duration before the inhibitor is added. Importantly, this analysis focuses on how these strategies affect the stability of inhibition once the inhibitor is no longer present.

2. Experimental

2.1. Materials

Commercial grade bare AA2024-T3 (Kaiser Aluminium, rolled thickness = 2 mm) was used as substrate. The substrates were embedded in epoxy to create electrodes with an exposed surface area of approximately 500×500 μm^2 [28,35,36]. A 0.05 M NaCl aqueous solution (>98 % purity NaCl in "Millipore Elix 3 UV" treated water) was used as the stock corrosive solution. This stock NaCl solution was further used to prepare a 1 mM $Ce(NO_3)_3$ + 0.05 M NaCl solution and a 45 mM Ce $(NO_3)_3$ + 0.05 M NaCl. The more concentrated Ce(III) solution was used for the delayed addition of the corrosion inhibitor (i.e., corrosion inhibitor is added to the system after a set time from the start of exposure).

2.2. Experimental protocols

Prior to immersion, the electrode surface was ground with SiC sandpaper from 320 to 4000 grit. They were then polished with 3 and 1 μm diamond paste. Pre-immersion SEM-EDX (JEOL JSM-7500F field emission scanning electron microscope coupled with energy dispersive X-ray spectroscopy) analysis was conducted on some electrodes to obtain location and initial composition of IMPs. The SEM-EDX was operated in back-scattered electron mode. The electrodes were repolished with 1 μm diamond paste and washed in an ultrasonic bath containing ethanol after pre-immersion SEM-EDX to remove any potential contaminants.

For the immersion tests, the electrodes were placed in reflected light microscopy setup composed of an electrochemical cell (redox.me Raman electrochemical flow cell) and a reflected microscope (Dinolite AM7515MT4A, ~10 pixel μm^{-2}) in brightfield illumination for in-situ acquisition of images of the surface during immersion [28,35]. Several immersion test variants were implemented to assess the impact of exposure duration to inhibitor solution and inhibitor supply delay on re-immersion stability. These variants are summarized in Table 1. The immersion test protocols can be divided into the tests with no supply delay and the tests with supply delay. The tests with no supply delay (i.e., UDxx) were supplied with Ce(III) from the start of the exposure using the 1 mM $Ce(NO_3)_3$ + 0.05 M NaCl solution. The samples were then kept immersed depending on the target total immersion time. For the tests

Table 1
Summary of immersion conditions used. Samples with no supply delay are identified as UDxx while samples with supply delay are identified as DSxx. The xx refers to the number of hours of immersion to the solution containing Ce(III).

Sample Code	Inhibitor supply time (s) with respect to start of exposure to 0.05 M NaCl	Total Immersion Time (h)
UD03	0	3
UD24	0	24
UD72	0	72
DS03	30	3

with supply delay (i.e., DSxx), 4.4 mL of the stock NaCl solution was first injected into the cell. A second solution consisting of 0.1 mL of the 45 mM $Ce(NO_3)_3$ + 0.05 M NaCl was then injected at 30 s from the start of exposure. Accurate determination of the start of exposure is possible with live images from the microscope during solution injection. After injection of the second solution, the net concentration of $Ce(NO_3)_3$ will be 1 mM. The samples were then kept in immersion for the target duration. Notably, the only immersion duration used for the tests with supply delay is 3 h.

After immersion, the samples were washed with deionized water and dried with a nitrogen stream. The samples were then reloaded into the reflected light microscopy setup for the subsequent re-immersion in 4.5 mL of 0.05 M NaCl. The same re-immersion protocol is applied for both the UDxx and the DSxx samples. Re-immersion was monitored for at least three hours and up to 24 h. Once re-immersion was completed, the samples were again washed with deionized water and dried with a nitrogen stream. Duplicate tests were performed for each immersion condition.

2.3. Image analysis

Brightfield reflected light microscopy observation of a polished AA2024 surface enables detection of pixel-level reduction in the intensity of light reflected back to the microscope (i.e., pixel darkening) due to surface processes such as dealloying, pitting, and oxide deposition, as discussed elsewhere [28,37]. The surface darkens because these surface processes scatter incident axial light, thereby reducing the amount reflected back to the detector. The image analysis protocol enables quantification of the pixel darkening by implementing image subtraction against a reference image. When applied to an image time series, the protocol can provide qualitative and quantitative information regarding the time dependence of the pixel changes and of their corresponding surface processes. It should be noted that image pre-processing (i.e., recursive re-alignment, image repositioning) was implemented prior to subtraction.

For the RM images from immersion, subtraction was performed with respect to an image obtained shortly before or at the start of immersion. For the RM images from re-immersion, subtraction was performed with respect to an image acquired at the start of re-immersion (i.e., image @ 0 s of re-immersion – image @ *x* s of re-immersion). The image subtraction generates the global activity map (GAM) for the sample at time x. A built-in ImageJ [38] look-up table (i.e., Fire) was used to recolour the GAMs to enable easier visualisation of the magnitude of the changes (i.e., activity level). Each pixel in the GAM has a corresponding activity level measured in a 0–255 scale, with 0 indicating no change with respect to the initial condition and 255 indicating the theoretical maximum pixel darkening. It is noted that the re-immersion GAMs only show degree of pixel darkening during re-immersion and do not depict the changes observed during the prior immersion period. Furthermore, the GAMs also constitute a time series, similar to the RM images from which they were derived.

Analysis of local activity evolution around certain sites (e.g., IMPs, active sites) in GAMs was performed by superimposing object borders. Object borders were extracted either from the pre-immersion SEM images or manually defined from the RM images. A bounding rectangle with a 4 pixel margin is then defined from the object borders to create rectangular regions of interest (RROI). The RROIs allow monitoring of activity on identified sites and their adjacent areas. Evolution of the activity of pixels in the RROI with time is summarized in terms of the median activity level (midAL) as previously introduced elsewhere [28]. At any given time, the individual pixels within RROI have their own activity levels. The midAL is the median of these individual pixel activity levels. It provides a semi-quantitative basis for assessing the extent of surface changes that occurred on the IMP surface and its adjacent matrix and also shows how the extent of surface changes evolve with time (Fig. 1). The median is preferred over other measures of central tendency because it is less sensitive to extreme values.

3. Results and discussion

3.1. Evolution of IMP surface during re-immersion

Local surface behaviour in the UD03 exposure condition was used as the base case for assessing the local loss of inhibition during re-immersion. The initial 3-hour immersion period for UD03 is characterized by reduced local corrosion activity in AA2024 exposed to a corrosive environment. This is highlighted by the minimal changes observed when comparing the electrode surface at 0 s (Fig. 2a) and after 10800 s (Fig. 2b) of immersion. Movie 1 shows a time-lapse of the surface changes between 0 and 10800 s. Notably, the IMPs shown in Fig. 2 and Movie 1 are grouped into S-phases (Al_2CuMg), θ-phases (Al_2Cu), and secondary particles ($(Al,Cu)_x(Fe,Mn)_ySi$ or AlCuFeMn) based on their EDX-derived compositions. Their boundaries are also color-coded based on these compositions (blue: S-phase, purple: θ-phase, green: secondary particle, yellow: unknown). In uninhibited systems, local corrosion processes such as dealloying, trenching, and corrosion product deposition lead to darkening of the surface [37]. However, with Ce(III), most of the surface remained bright during immersion, except for some S- and θ-phase particles. In our previous work [28], we have shown that the pixel darkening and its corresponding activity level correlates to Ce(III)

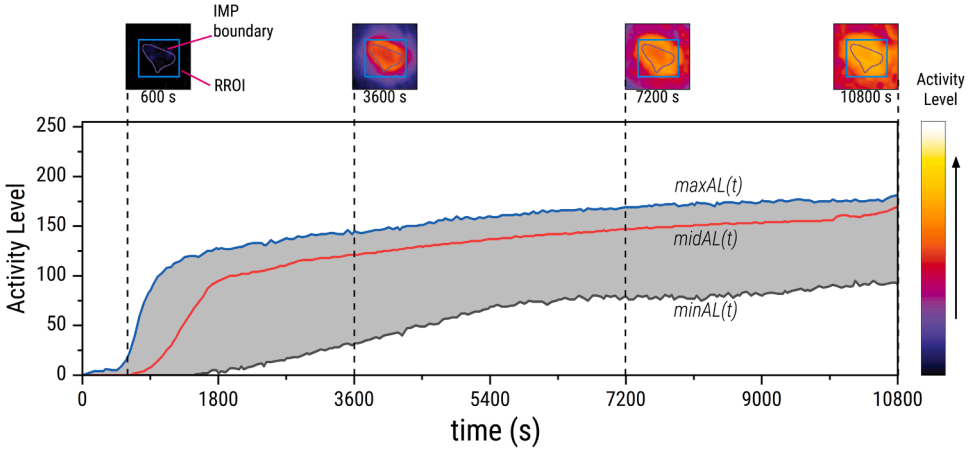

Fig. 1. The activity level of individual pixels on the intermetallic particle (IMP) surface and its adjacent matrix (i.e., pixels within the RROI) can be summarized in terms of the maximum (maxAL), median (midAL), and minimum (minAL) activity level. The evolution of these parameters with time provides a semi-quantitative basis for analysing the kinetics of local surface changes.

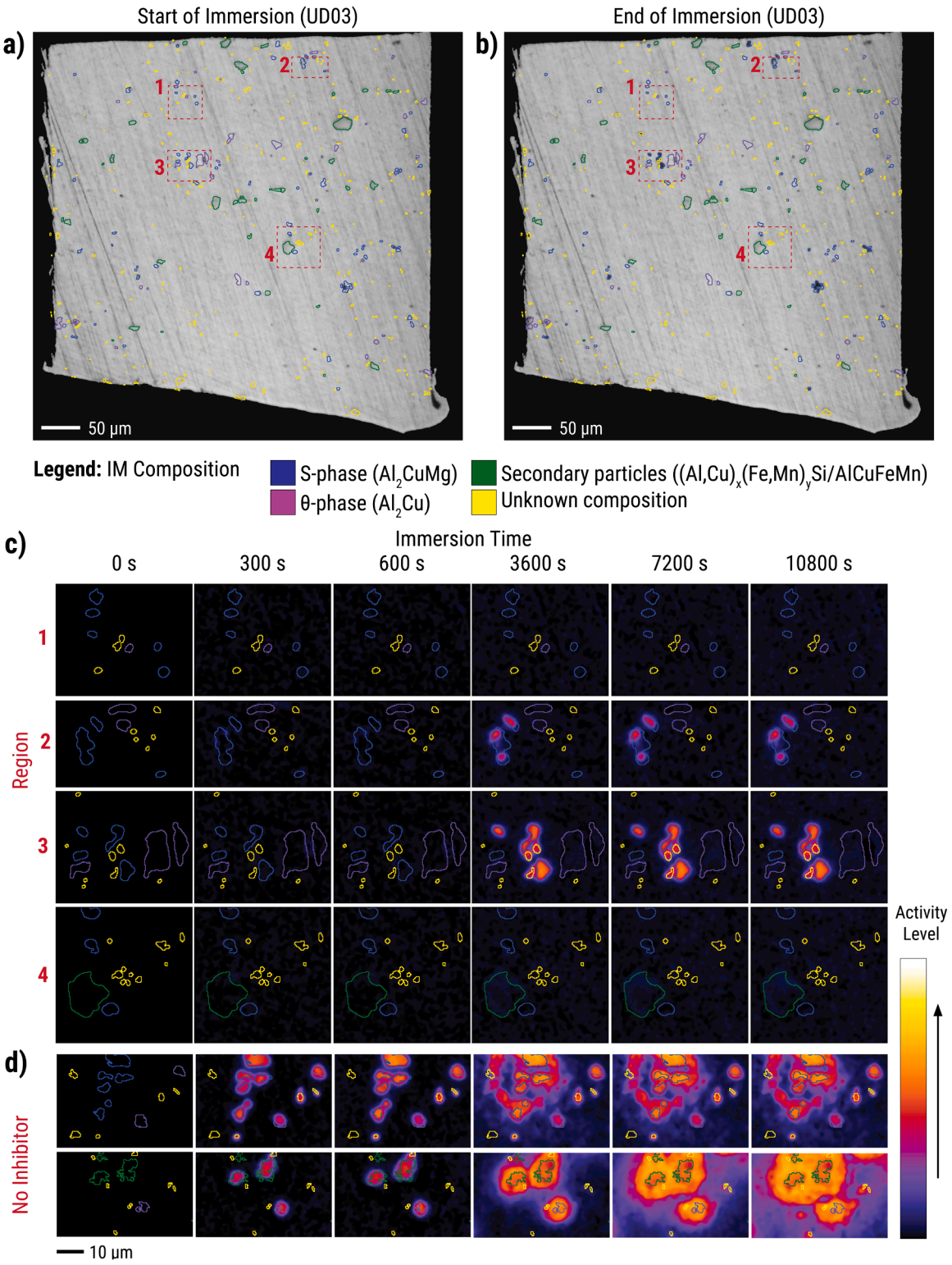

Fig. 2. Reflected light microscopy images show the condition of a UD03 sample surface (a) at the start, and (b) at 10800 s of immersion in 0.05 M NaCl with 0.001 M $Ce(NO_3)_3$; (c) UD03 immersion activity maps at different times highlight the progression of surface changes during exposure to the inhibitor and show that they are minimal compared to (d) activity maps from sample immersed in just 0.05 M NaCl.

precipitation on the IMP surface. Fig. 3 shows examples of IMPs from our previous work with varying degrees of activity after 3 h of immersion in 0.05 M NaCl containing 0.001 M $Ce(NO_3)_3$. In Fig. 3a, particles were exposed to Ce(III) immediately when immersion began, while in Fig. 3b and Fig. 3c, Ce(III) was introduced 60 s after the start of immersion. The activity maps and their corresponding post-immersion back-scattered electron images highlight that higher activity levels is related to more extensive Ce(III) precipitation (i.e., thicker inhibiting layers). This relationship is fundamental in the succeeding analysis of the activity maps obtained from the immersion and re-immersion tests.

Local activity maps in Fig. 2c provide a closer look at the activity evolution of particles that maintained low activity (Region 1 and Region

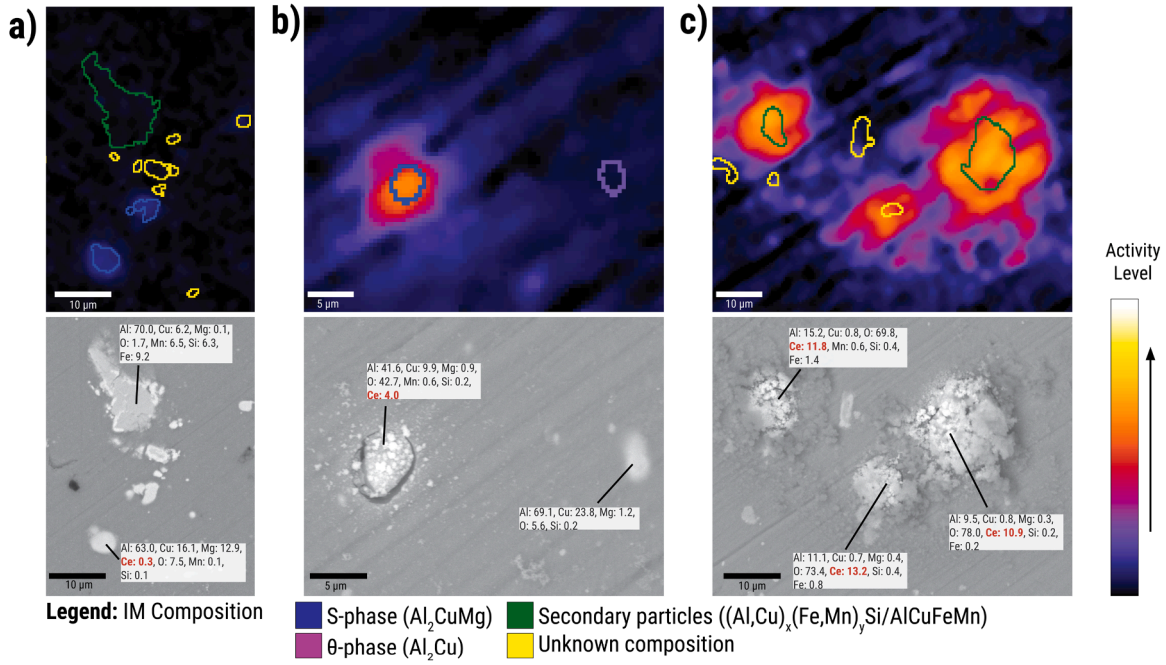

Fig. 3. Examples of IMPs with (a) low activity level, and (b, c) high activity level at the end of 3 h of immersion in Ce(III)-containing solution. The post-immersion backscattered electron images show the degree of Ce(III) precipitation corresponding to the activity. The particles shown are part of the results from [28].

4) and of particles that developed high activity (Region 2 and Region 3). Activity maps of Regions 1 and 4 show little changes during the three-hour immersion in the Ce(III)-containing electrolyte. No warm-coloured pixels were observed, and the activity of the pixels within the IMP boundaries remained comparable to the matrix. Given that most of the IMPs in these two regions are S- and θ-phases, the absence of high activity likely indicates inhibition from Ce(III). Undetectable changes further suggest the Ce(III)-inhibiting layer has very low thickness. In Regions 2 and 3, IMP activity was observed between 600 and 3600 s. This is significantly much later than the appearance of activity in un-inhibited particles (Fig. 2d). The activity started on the IMP surfaces and did not spread to the surrounding matrix. By the end of immersion, the surfaces have activity levels in the orange to yellow-orange range of the activity colour scale. The observed changes were slower, more limited, and less extensive than those in NaCl-only solutions (Fig. 2d), where dealloying and trenching occurred. These results are in line with our previous reports on delayed inhibitor supply where we showed how Ce-based inhibiting layers become more substantial when there is dealloying prior to inhibitor addition [28]. The fact that some IMPs showed more Ce deposition than others indicates that some IMPs were dealloyed before immersion, likely due to some degree of atmospheric corrosion due to condensation on IMP surfaces prior to exposure to the electrolyte (Supporting Information 1).

Fig. 4 shows the changes of the electrode first shown in Fig. 2a,b during its re-immersion in 0.05 M NaCl. Movie 2 shows a time-lapse of the surface changes between during this re-immersion period. Fig. 4a and Fig. 4b show the appearance of the surface at 0 s and after 10800 s of re-immersion, respectively. The two images show high degree of changes once the inhibitor is not present in the system anymore. Fig. 4c shows a closer look at the regions shown in Fig. 2c during re-immersion. As during immersion, the IMPs exhibit either low (Region 1 and 2) or high (Region 3 and 4) activity.

Supplementary material related to this article can be found online at doi:10.1016/j.corsci.2025.113146.

Region 1 (Fig. 4c) shows particles which exhibited low activity during immersion (Fig. 2c, Region 1). During re-immersion, the onset of activity (i.e., appearance of purple pixels) was observed on the IMP surface some time between 300 and 600 s of re-immersion. The activity gradually extended to the adjacent matrix, marked by the slow-spreading purple area from 600 to 10800 s (see white arrows in 3600–10800 s frames in Fig. 4c, Region 1). The activity level of the pixels on and around the IMPs remained low, nonetheless, at the end of the observed period.

Region 2 (Fig. 4c) contains two S-phase particles (s1 and s2; EDX spectra provided in Supporting Information 2) that showed visible activity localized on the IMP surfaces during immersion (Fig. 2c, Region 2). The rest of the particles in this region exhibited low activity during immersion. The particles s1 and s2 showed minimal (light purple) activity during re-immersion. The activity started somewhere between 0 and 300 s on the matrix adjacent to the IMPs. It apparently stopped between 600 and 3600 s, as no significant activity changes were seen after 3600 s. Notably, segments of the surfaces of s1 and s2 which showed visible activity during immersion exhibited minimal activity during the re-immersion. This does not necessarily mean no further changes occurred on or under these areas since the current microscopy setup can only detect changes that further increase light scattering on the sample surface (e.g., additional deposition, significant inhibiting layer dissolution). Nonetheless, since activity on the adjacent matrix remained very low at 3 h of re-immersion, activity of the inhibiting layer or the underlying particle are most likely very limited.

Region 3 (Fig. 4c) contains three S-phase particles (s3, s4, and s5; EDX spectra provided in Supporting Information 2) that exhibited visible activity during immersion (Fig. 2c, Region 3). During re-immersion, activity developed between 0 and 300 s on the matrix adjacent to these particles, spreading further with time. After 3 h of re-immersion, the adjacent matrix of s4 and s5 showed high activity levels (i.e., orange-colored pixels) while s3 activity levels remained on the lower end. The IMP surface of s4 and s5 also exhibited some activity after three hours of re-immersion, indicating potential changes on the inhibiting layer that formed on the surface during immersion.

Meanwhile, the θ-phase IMPs (t1 and t2; EDX spectra provided in Supporting Information 2) which exhibited low activity during immersion (Fig. 2c, Region 3) became active between 0 and 300 s of re-immersion. The re-immersion activity initiated from the defect between the two particles which was present even prior to the immersion period (Supporting Information 3). After 3 h of re-immersion, the matrix

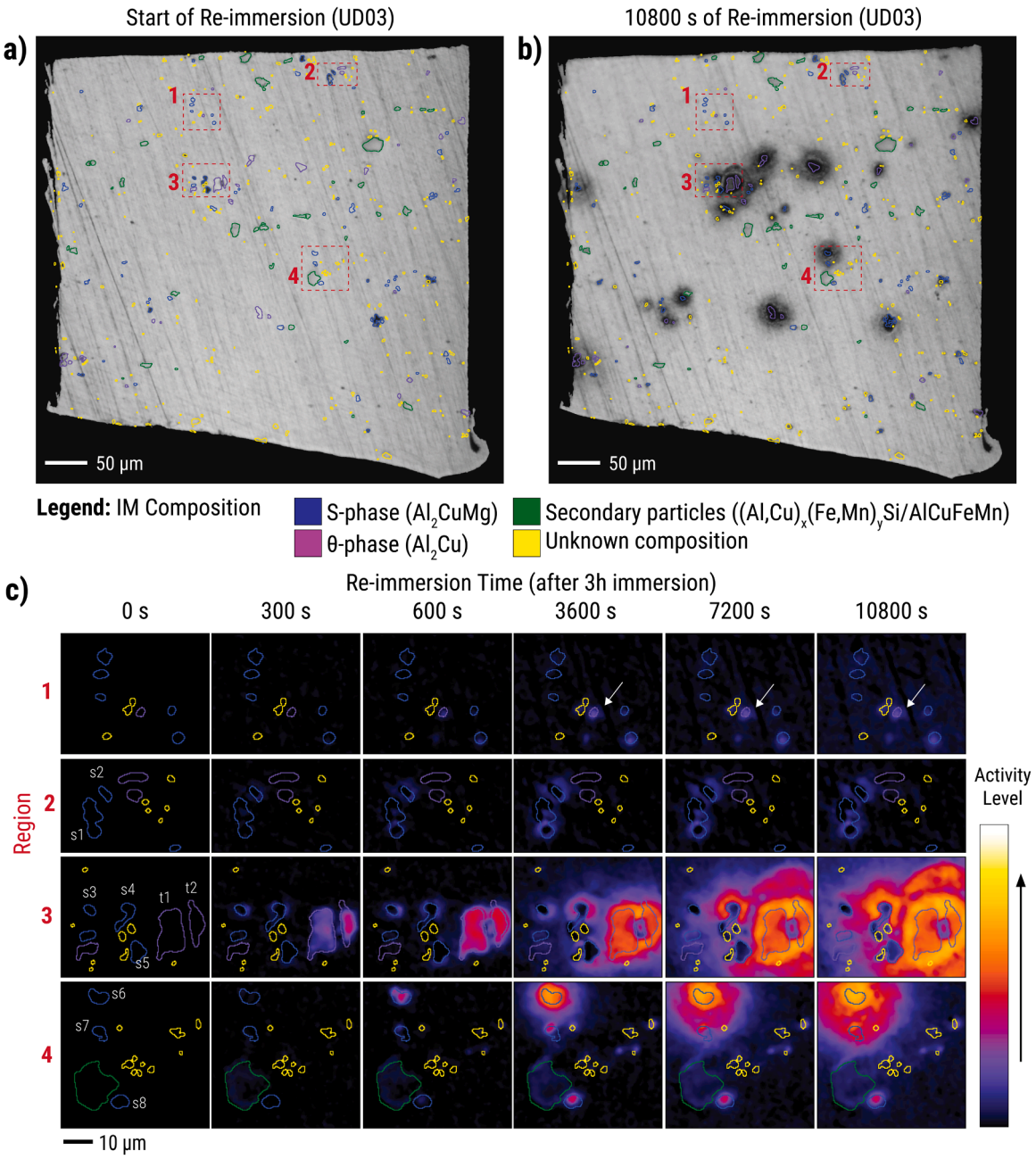

Fig. 4. Reflected light microscopy images of a UD03 sample (a) at the beginning, and (b) at 10800 s of re-immersion in 0.05 M NaCl; (c) UD03 re-immersion activity maps from selected regions of the sample surface show the local onset and progression of inhibition loss.

surrounding the particles developed higher activity (i.e., yellow pixels) than the IMP surfaces (i.e., red-orange pixels). This spatial distribution of activity is consistent with a dealloyed particle surrounded by a massive trench [28].

Region 4 (Fig. 4c) shows S-phase IMPs (s6, s7, s8; EDX spectra provided in Supporting Information 2) which had low local activity during immersion. During re-immersion, their activity initiated on the IMP surfaces between 300 and 600 s. This eventually spread to the adjacent matrix from 600 s and continued with further re-immersion. The particle s6 exhibited the most extensive changes on its adjacent matrix.

Fig. 4c shows that during re-immersion in 0.05 M NaCl, the loss of inhibition for AA2024 after 3 h of immersion in Ce(III)-containing electrolyte still starts at the IMPs, similar to uninhibited systems. Notably, there is variability in the IMP inhibition even among particles of the same composition. This variability is more apparent when the immersion/re-immersion behaviours of the IMPs sampled from two replicates (total number of sampled IMPs = 901) are taken into consideration. Fig. 5a shows the midAL values at the end of the 3 h re-immersion in inhibitor-free corrosive solution (y-axis) versus the midAL values after the initial 3 h immersion to the Ce(III)-containing solution (x-axis). Along the x-axis, most particles have midALs close to 0 while a smaller group have midALs above 25. These two groups constitute the low and high activity groups during immersion. To classify the particles quantitatively, a midAL threshold of 20 is used to separate IMPs with low and high midALs. The value is based on the visual clustering of the midALs and on the threshold used by Olgiati et al. [37] for identifying active pixels. The same threshold is applied for the classification of re-immersion behaviour. Sites that exhibited midAL ≤ 20 are categorized as having L-type behaviour and those with midAL > 20 as having H-type behaviour. Fig. 5a includes vertical and

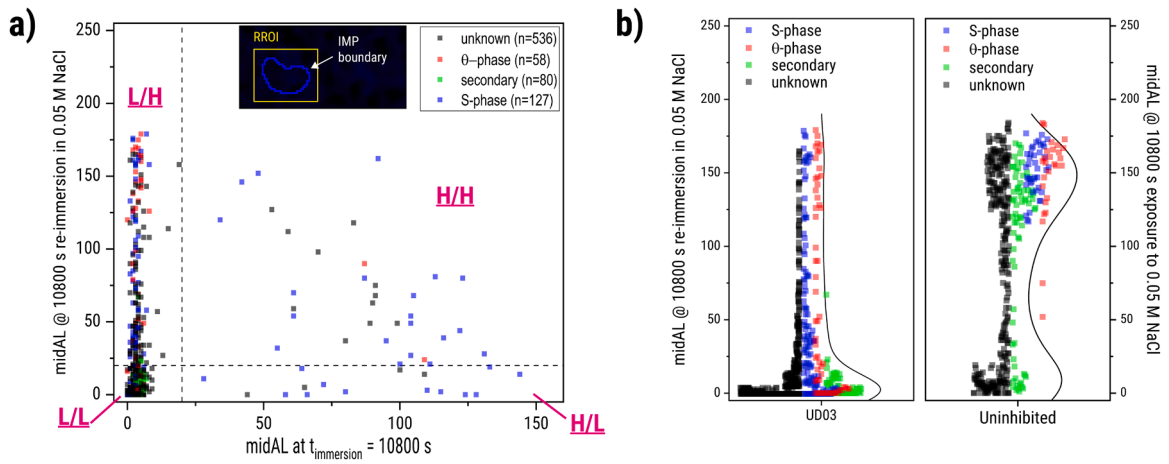

Fig. 5. Analysis of the local changes during re-immersion of the UD03 sample in 0.05 M NaCl expressed in terms of (a) midAL during re-immersion correlated with the midAL during immersion in 0.05 M NaCl + 0.001 M $Ce(NO_3)_3$ (inset shows example of an RROI used to measure midAL), and (b) comparison of midALs of UD03 IMPs after 3 h re-immersion in 0.05 M NaCl and midALs of uninhibited IMPs during a 3 h exposure to the same electrolyte.

horizontal dashed lines at the threshold value, dividing the plot into four zones corresponding to the combinations of immersion and re-immersion behaviours: *L/L* (low activity in immersion and low activity in re-immersion), *H/L* (high activity in immersion and low activity in re-immersion), *L/H* (low activity in immersion and high activity in re-immersion), and *H/H* (high activity in immersion and high activity in re-immersion). These zones align with the optical observations in Fig. 2c and Fig. 4c.

The immersion/re-immersion behaviour distribution (Fig. 5a) shows that majority of the particles (72.6 %) are in the L/L zone. This includes almost all of the EDX-confirmed secondary particles (i.e., IMPs whose compositions were confirmed to be that of secondary particles through EDX) and some S- and θ-phase IMPs. Around 1.4 % of the particles, mostly S-phase IMPs, were in the H/L zone. The spread in the immersion midALs of the IMPs in this zone indicates that stable inhibition can be achieved with varying degrees of Ce(III) precipitation. Around 3.2 % of the IMPs, also predominantly S-phases, are in the H/H zone. There is also a visible spread in the immersion midAL of the IMPs in this zone. A lower re-immersion midAL is observed though for particles with higher immersion midAL. The rest of the particles (~22.7 %) are in the L/H zone. IMPs with EDX-confirmed compositions in this group were also S- and θ-phases. The particles in this zone exhibit visible spread in the re-immersion midAL values. Furthermore, the most active particles during re-immersion are in this zone.

Although the presence of IMPs in the H/H and L/H zones indicates inhibition failure the initial exposure to Ce(III) still contributed to a lower frequency of active IMPs during re-immersion in 0.05 M NaCl relative to a system that is only exposed to NaCl. This is evident from comparing the midALs (Fig. 5b) of UD03 IMPs after 3-hours of re-immersion in 0.05 M NaCl against those of the uninhibited IMPs after 3-hours of exposure to 0.05 M NaCl (i.e., without prior immersion in Ce (III)-containing electrolyte). The midAL distribution for the uninhibited IMPs shows two maxima, a low midAL maxima between 0 and 25, and a high midAL maxima between 125 and 175. The high midAL maxima is not observed among the UD03 IMPs during their re-immersion. Furthermore, the distribution also highlight a change in the IMP compositions comprising the low midAL maxima. In the uninhibited system, this low midAL maxima is dominated by EDX-confirmed secondary particles. However, in the re-immersed UD03 samples, S- and θ-phase IMPs are observed to contribute to this maxima. This is a clear indication that more S- and θ-phase exhibit reduced activity when initially exposed to the inhibitor. Altogether, the IMP midAL values for the re-immersion of UD03 and for the uninhibited immersion suggests that some of the inhibition is retained even when the inhibitor is not available in the solution anymore. Otherwise, the UD03 IMPs would have just behaved similar to the uninhibited IMPs. It is also interesting to note that secondary particles, which usually interact less with Ce(III) compared to S- and θ-phases [14], actually show the biggest difference in the number of highly active IMPs when comparing UD03 re-immersion and uninhibited conditions (Fig. 5b). For the uninhibited IMPs, secondary particles also contribute to the high midAL maxima. However, during the re-immersion of UD03, almost all of the EDX-confirmed secondary particles are found on the low midAL maxima.

3.2. *Immersion/re-immersion behaviour subtypes and proposed mechanisms*

From the activity maps in Fig. 4c and the immersion/re-immersion zones identified in Fig. 5a, subtypes of the four general immersion/re-immersion behaviours (i.e., L/L, H/L, L/H, H/H) have been further identified particularly when the long-term re-immersion behaviour is considered. Examples of each subtype are presented in Fig. 6 and potential mechanisms that explain each specific behaviour are as follows:

- **L/L (low activity in immersion and low activity in re-immersion):** Two subtypes of the L/L behaviour have been identified. The first involves minimal changes on the IMP surface and its surroundings even at prolonged re-immersion (L/L-A). The second involves IMPs with surfaces that remain clear despite extensive corrosion product deposition or matrix dissolution on its surroundings at prolonged re-immersion (L/L-B).

  The L/L-A behaviour indicates that the surface is largely inactive. Fig. 6a shows an example of an AlCuFeMn IMP that exhibits this behaviour. No signs of activity during immersion, and minimal changes during the 3 h re-immersion were observed in the particle's RROI. The pixels on the IMP surface exhibited a slightly higher activity level than the adjacent matrix with further re-immersion (see Fig. 6a - 6 h). Further increase of the pixel activity on the IMP surface was not observed with further re-immersion. The hazy purple patch observed at 20 h is due to corrosion product deposition from nearby sites. The activity propagation started from the bottom left corner of the map and moved towards the top right corner (Supporting Information 3). The propagating patch indiscriminately covered the IMP and its adjacent matrix which suggests a uniform lack of activity on the area. Such IMP inactivity is attributed to the IMP's low susceptibility to dealloying. During immersion, minimal dealloying leads to limited Ce(III) precipitation on the IMP surface and thus low activity [14,28]. During re-immersion, minimal dealloying also

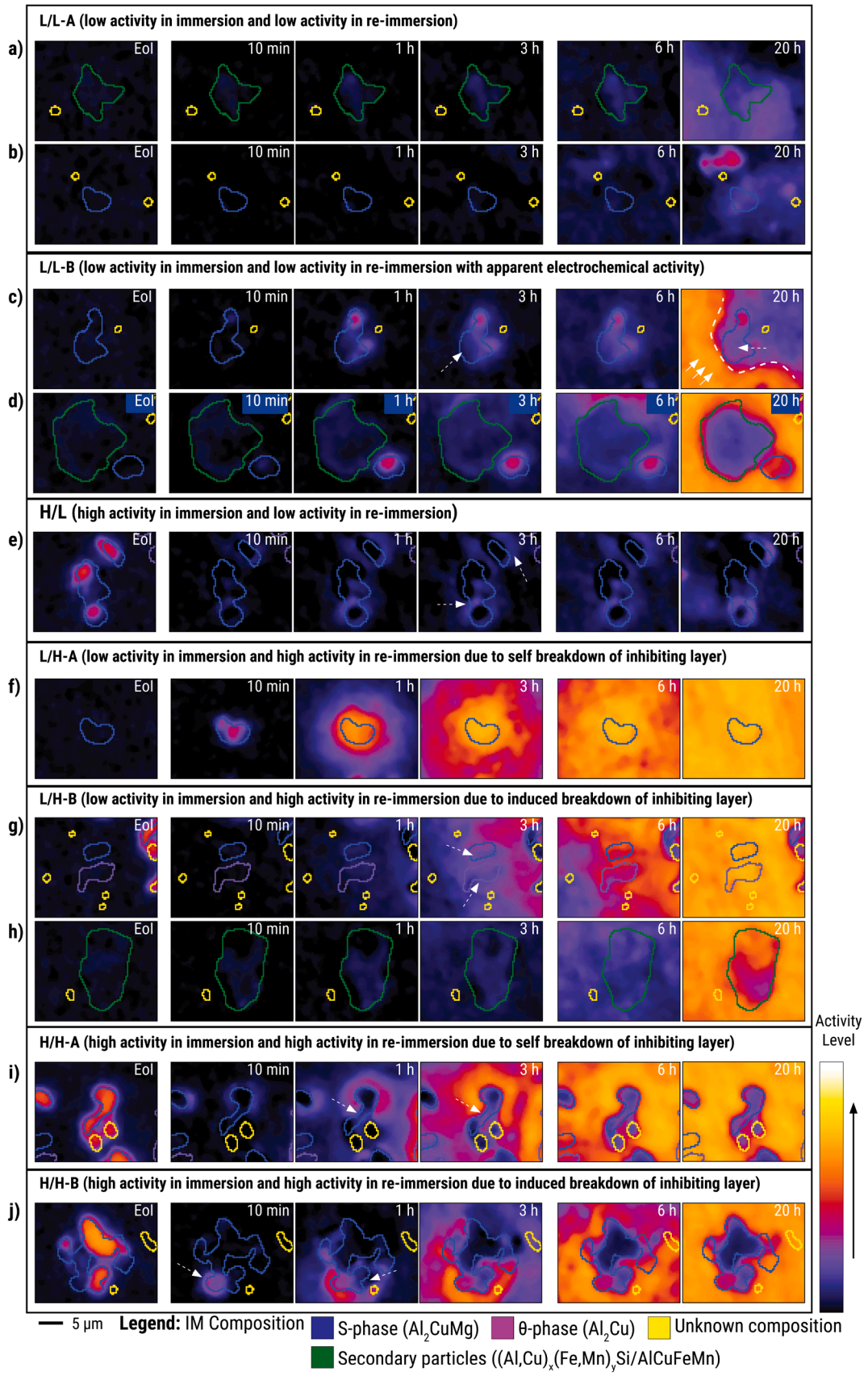

Fig. 6. Examples of immersion/re-immersion behaviours subtypes: (a, b) low/low (L/L) behaviour, (c, d) L/L behaviour and apparent electrochemical activity, (e) high/low (H/L) behaviour, (f) low/high (L/H) behaviour, (g, h) L/H behaviour induced by nearby corroding sites, (i) high/high (H/H) behaviour, and (j) H/H behaviour induced by nearby corroding site. 'EoI' pertains to end of immersion in 0.05 M NaCl + 0.001 M $Ce(NO_3)_3$ for 3 h.

results to limited local corrosion observed as low activity on the IMP surface. This mechanism potentially accounts for the behaviour of certain subtypes of secondary particles (e.g., $Al_{20}Cu_2Mn_3$, $Al_{76}Cu_6Fe_7Mn_5Si_6$) that have been consistently reported to be less prone to dealloying [14,39].

Apart from stability because of IMP composition, L/L-A behaviour can also be attributed to non-exposure of the particle due to stable material layer covering the surface. This can account for the lack of changes in some of the conventionally active S- and θ-phases. Fig. 6b shows an example of an S-phase IMP with this behaviour. Minimal activity was observed on the IMP's RROI during immersion which makes formation of a thick inhibiting layer less likely. The IMP was also minimally active during the first 3 h of re-immersion and further re-immersion only lead to indiscriminate deposition of corrosion products (e.g., $Al(OH)_3$) from nearby particles resulting to a hazy purple patch. Several mechanisms could have generated the stable layer. It could be an oxide layer formed during exposure to the corrosive solution. SKPFM studies of AlCuMg particles by Lacroix et al. [40,41] showed that oxides can form on top of particles during exposure to corrosive electrolyte. It could also be an inhibiting layer formed from Ce(III) precipitation. In our earlier work, small amounts of Ce was detected on the surface of IMPs following immersion in conditions similar to UD03 [28].

The L/L-B behaviour also involves IMPs which exhibited minimal activity during the 3 h of immersion and during the first 3 h of re-immersion. However, when surrounding matrix dissolution and corrosion product deposition became substantial with prolonged re-immersion, particles in this subtype exhibit IMP surfaces that remain relatively bright. Fig. 6c shows an example of an S-phase particle (EDX spectra provided in Supporting Information 2) with this specific behaviour. The particle exhibited minimal activity during immersion despite its composition which suggests that a thin inhibiting layer is present. During re-immersion, visible activity developed at the top and right-most sections of the IMP surface between 600 and 3600 s of exposure to the saline environment. The activity on the surface remained relatively low (purple to violet in the colour scale) even at 3 h of re-immersion (see arrow in Fig. 6c – 3 h). The sustained low activity suggests that some form of inhibiting layer breakdown occurred. The breakdown appears to be contained though as the IMP surface did not show extensive activation typical of dealloying particles (Fig. 2d). Corrosion product deposition from nearby corroding sites led to a propagating active area on the surrounding matrix of the particle. The propagating area had low activity (i.e. purple in the colour scale) at 6 h. Extensive cooperative corrosion of neighbouring sites eventually led to spreading matrix dissolution observed as high activity at 20 h (i.e., red-orange in the colour scale). The front of the propagating area, which was moving towards the top right direction, apparently avoided the S-phase IMP (see dashed line in Fig. 6c – 20 h). The surface of the IMP is also partially covered by corrosion products, but the coverage appears to be less extensive as indicated by its lower activity levels (see arrow in Fig. 6c – 20 h) compared to the adjacent matrix at the top left and bottom right of the particle (i.e., points along the front of the propagating active area). Fig. 6d shows a similarly intact surface of an AlCuFeMnSi particle surrounded by extensive matrix dissolution during re-immersion. The dissolution was also triggered by neighbouring active IMPs.

The bright IMP surfaces (i.e., low-activity surfaces) suggest that the IMPs are neither significantly dealloyed nor buried under corrosion products. An intact IMP indicates minimal dealloying while the absence of a corrosion product cover suggests that their surface pH (i.e., either very low or very high) does not support aluminium hydroxide deposition [42]. High pH-driven dissolution of aluminium hydroxide (i.e., $Al(OH)_3$ is converted to $Al(OH)_4^-$) is considered more likely as the intact IMP surface can facilitate cathodic reactions (i.e., oxygen reduction reaction) which generate hydroxide ions. Cathodic activity in the absence of substantial dealloying is within expected behaviour for Fe-rich secondary particles [14,39]. However, for S-phases, cathodic activity is typically accompanied by extensive dealloying. As such, the observation of low-level IMP activity that did not progress to full dealloying with signs of cathodic behaviour may indicate the effect of the inhibiting layer. Previous works [12,14,28] have shown that slight dealloying can form a thin inhibiting layer which can isolate the underlying IMP during immersion. During re-immersion, small regions of the IMP surface not covered by the inhibiting layer could potentially enable cathodic reactions to proceed on the IMP surface. The presence of the inhibiting layer, nonetheless, prevents extensive dissolution of Al and Mg. Confirmation of the S-phase surface microstructure that leads to this behaviour is recommended for future works.

Depending on the aggressiveness of the corrosion of neighbouring sites, particles that initially showed L/L-A or L/L-B behaviour may eventually be activated and exhibit L/H behaviour (see L/H section). Additionally, since L/L-B behaviour is identified based on matrix dissolution and corrosion product build-up, some L/L-A sites situated away from major matrix damage might be undetected L/L-B sites. Nonetheless, based on the surface activity after about 20 h of re-immersion, *at least* 23 of the 153 L/L particles with EDX-confirmed compositions (~14 %) were classified as L/L-B (Supporting Information 4).

- **H/L (high activity in immersion and low activity in re-immersion):** As presented in Fig. 4, IMPs with H/L behaviour exhibited high activity during immersion and low activity during re-immersion. Fig. 6e shows S-phase particles with this behaviour. These are the same S-phase particles (s1 and s2) shown in Fig. 4c. Both particles exhibited activity development on the adjacent matrix, around the precipitation sites from immersion. The activity slightly exceeded the threshold value of 20 in some places (see arrows in Fig. 6e – 3 h). Nonetheless, the overall RROI activity remained low the during the 3 h re-immersion, and even with further re-immersion to 20 h.

  High activity during immersion is attributed to IMP dealloying which facilitated the formation of a thick Ce(III) inhibiting layer [28]. The formation of the layer is generally slow when the inhibitor is available from the start of exposure but prior partial dealloying can lead to faster precipitation [28]. This prior dealloying is only observed in a limited number of the sampled particles (~1.4 %) and is likely due to partial corrosion introduced during the sample preparation step or atmospheric corrosion prior to exposure to the electrolyte. During re-immersion, the inhibiting layer slows down oxygen transport and Cu redistribution resulting to the low activity on the IMP surface and on the adjacent matrix. Changes around the adjacent matrix indicate trenching due to micro-galvanic coupling with the corroding IMP underneath the inhibiting layer. This suggests that there are defects (e.g., cracks, pores) in the inhibiting layer. The defects are not extensive though as the layer still provides considerable protection based on the slow growth of the trenches and their corresponding low-level activity.
- **L/H (low activity in immersion and high activity in re-immersion):** Two subtypes of the L/H behaviour were identified. The first subtype involved IMPs with low activity during immersion and exhibited self-breakdown of their inhibiting layers during re-immersion (L/H-A). The second subtype (L/H-B) also involved low immersion activity but had induced inhibiting layer breakdown due to activity of neighbouring particles. It is noted that processes that lead to low activity during immersion are expected to be similar to those seen for L/L behaviour – either the particle is inherently stable, or the particle had a stable thin layer that covered it and prevented further local corrosion.

  Fig. 6f shows an S-phase (same as s6 in Fig. 4c) that exhibited L/H-A behaviour. The particle activated within 10 mins of re-immersion but the activity remained concentrated on the IMP surface (Fig. 6f –

10 min). This spread is slower than those of uninhibited IMPs (Fig. 2d) and is consistent with loss of inhibition as opposed to absence of inhibition. Moreover, the activation time is also earlier than that of the L/L-B S-phase (Fig. 6c). This behaviour is attributed to failure of the thin inhibiting layer that protected the material during immersion. The inhibiting layer's susceptibility is attributed either to limited coverage of the IMP surface or presence of defects (e.g., cracks, pores) [14]. Both scenarios lead to a portion of the IMP surface exposed to the corrosive re-immersion environment. Since the exposed area is smaller than that of an uninhibited particle, the rate of Mg or Al dissolution as well as the rate of oxygen reduction reaction are expected to be lower leading to the relatively slower IMP activation.

It is noted that the L/H-A behaviour can also be explained by the breakdown of a passive layer (e.g., thin alloy layer or an alumina layer on top of the IMP surface) initially present on the IMP surface [40]. The passive layer can prevent IMP interaction with the corrosion inhibitor resulting to low activity during immersion. Breakdown of the passive layer during re-immersion can then lead to corrosion of the IMP and high re-immersion activity levels. Distinguishing an L/H-A scenario due to a passive layer from one due to a thin inhibiting layer requires non-destructive determination of the presence of the passive layer prior to immersion or re-immersion. Particles with such a substantial passive layer are expected to dealloy much later, if at all, in uninhibited conditions. Kinetic studies on the dealloying of S-phases in inhibitor-free NaCl solutions [28,37] showed that particles with delayed dealloying are not common. As such, attributing L/H-A behaviour to failure of thin inhibiting layers formed during immersion is considered more likely.

The L/H-B behaviour involves failure of a stable thin inhibiting layer due to induced activity from a neighbouring active sites. Fig. 6g shows particles which are candidates for the L/H-B mechanism. These S- and θ-phase particles (EDX spectra provided in Supporting Information 2) had minimal activity during immersion and did not show signs of IMP activation within the first hour of re-immersion. At 3 h of re-immersion, corrosion product from nearby corroding particles partially covered the IMP surfaces. However, some IMP areas remained free from corrosion products (see arrows in Fig. 6g – 3 h) similar to the particles in the L/L-B mechanism (Fig. 6c). With prolonged re-immersion, matrix dissolution also became more substantial leading to the activity intensification observed on the surrounding matrix (Fig. 6g – 20 h). The surfaces of the S- and θ-phase particles still exhibited lower activity but eventually reached the same level as the adjacent matrix at around 20 h. This equalization of activity is attributed to dealloying of the IMP surfaces which suggests complete loss of inhibition of the particles. Induced activity of the particles can be due to redistributed Cu particles weakening the inhibiting layer through nano-galvanic coupling [43, 44] or matrix dissolution leading to exposure of buried portions of the protected IMP [45].

This mechanism can also be extended to induced failure of inherently stable IMPs. The secondary particle in Fig. 6h (EDX spectra provided in Supporting Information 2) is a potential candidate for this. The lower section of the particle maintained its low activity but the upper section eventually showed signs of high activity attributed to dealloying at around 20 h of re-immersion. The induced activation of inherently stable particles is very limited as it was only observed with this IMP.

Since L/H-B behaviour requires influence of neighbouring sites, the fraction of particles with confirmed L/H-B behaviour during the first 3 h of re-immersion is only around 9 of the 87 L/H particles with EDX-confirmed compositions (~10 %) (Supporting Information 4). All of these L/H-B events occurred in areas with high IMP density. Thus, majority of the L/H behaviour documented is still from the self breakdown of inhibition. It is noted though that the L/H-B fraction is expected to increase if the analysis duration for re-immersion is also increased.

- **H/H (high activity in immersion and high activity in re-immersion):** Processes that lead to high activity during immersion are similar to those in IMPs with H/L behaviour (i.e., formation of a thick inhibiting layer). As with the L/H behaviours, two subtypes of the H/H behaviour have been identified: particles which undergo self-breakdown of the inhibiting layer (H/H-A), or particles whose breakdown is induced by neighbouring activity (H/H-B).

  Fig. 6i shows an S-phase particle (EDX spectra provided in Supporting Information 2) that shows activity evolution consistent with H/H-A. The IMP showed activity consistent with the formation of a thick inhibiting layer during immersion (Fig. 6i - EoI). During re-immersion, the IMP exhibited activity development between 10 min and 1 h of re-immersion on the matrix adjacent to the top section of the particle which suggests trenching. Between 1 and 3 h, visible activity increase on the middle section of the IMP surface (see arrow in Fig. 6i – 1 h, 3 h) suggests destabilization of the inhibiting layer on that area. Matrix dissolution and corrosion product deposition around the IMP also intensified based on the orange-level activity on the surrounding matrix. With prolonged re-immersion, activity increase on the IMP surface attributed to further corrosion product build-up is observed (pale purple at 20 h). The H/H-A behaviour is potentially due to inhibiting layer defects that exposed the underlying IMP to the corrosive solution. The corrosion of the IMP triggered the dissolution of the adjacent matrix and led to trenching around the IMP. This is observed as circumferential activity of the IMP.

  Fig. 6j shows a composite particle with partial thick deposition on some sites after immersion which exhibited H/H-B behaviour. Local corrosion of the unprotected sites at the bottom left section (see arrow in Fig. 6j – 10 min) led to potential destabilization of the inhibiting layer on the bottom right section of the particle. At 1 h re-immersion, activity attributed to inhibiting layer dissolution developed around the bottom right section (see arrow in Fig. 6j – 1 h). Further re-immersion lead to visible trenching around the composite particle and subsequent corrosion product deposition on the surrounding matrix. As with the L/H-B behaviour, the H/H-B behaviour is likely due to the influence of nearby corroding particles. These IMPs can induce dissolution of the aluminium matrix which can then expose buried sections of the protected IMP and trigger local corrosion propagation [45]. Around 2 of the 17 H/H particles with EDX-confirmed compositions (~12 %) exhibit H/H-B behaviour (Supporting Information 4).

Given the observed variability in behaviour amongst IMPs, a corrosion strategy based on the IMPs most susceptible to inhibition-loss can be a viable approach. Arguably, the IMPs which exhibit L/L and H/L behaviour (~74 % of sampled IMPs) do not pose considerable risk as their protection is maintained during re-immersion. A good number of these particles are also likely to be inherently stable so leaving them to behave as they do seems to be acceptable. The particles which exhibit high activity during re-immersion need more attention as they can induce local corrosion of protected neighbours which can then lead to cooperative corrosion with prolonged re-immersion. Between H/H and L/H behaviour, the L/H IMPs have a higher incidence rate (~22.7 % of sampled IMPs) and exhibited more extensive activity during re-immersion. Taking these observations together, using a strategy that reduces the number of IMPs showing low interaction with the inhibitor can potentially lead to more stable protection during re-immersion. In the case of Ce(III), this can be achieved by increasing the degree of Ce (III) precipitation on the IMP surface.

3.3. Effect of inhibiting layer formation conditions on inhibiting layer stability during re-immersion

Exposure to Ce-containing inhibiting solutions has been reported to increase corrosion protection with longer immersion time due to thicker inhibiting layers formed and larger surface areas covered [14,46–48]. The increase in protection supports existing preference for sustained inhibitor release in active corrosion protection systems. Time-dependent growth of the inhibiting layer is attributed to permeation of corrosive species which can lead to gradual dealloying-driven precipitation of Ce [14]. This layer growth is observed when the global activity maps of AA2024 samples exposed to 0.05 M NaCl + 0.001 M Ce(III) for 3 h (UD03), 24 h (UD24), and 72 h (UD72) are compared (Fig. 7). Movie 3 and Movie 4 show time-lapses of the surface changes between for UD24 and UD72, respectively, during their re-immersion in 0.05 M NaCl. As can be seen in the activity maps at end of immersion (EoI), UD24 (Fig. 7b) and UD72 (Fig. 7c) both appear to have higher number of active sites with higher activity (orange in the colour scale) compared to UD03 (Fig. 7a). Note that the edge activity in the UD72 EoI map is due to microscope focus changes during imaging, not precipitation events. Comparison of the end-of-immersion activity maps of the test replicates show comparable degrees of precipitation and number of active sites for UD03 (Fig. 7a, Fig. 8a) and UD72 (Fig. 7c, Fig. 8c). The UD24 replicates (Fig. 7b, Fig. 8b) on the other hand have a visible difference in the number of active sites. This is potentially due to the variation in IMP make-up of the two tests [49]. It also suggests that a consistent increase in inhibiting layer growth is not yet achieved with a 24-hour immersion duration. Nonetheless, re-immersion behaviour of the replicates in Fig. 8a-c (Supporting Information 5) are consistent with those shown in Fig. 7. It is noted that the activity that develops during re-immersion is consistent with local corrosion, as confirmed by post-re-immersion secondary electron images in Fig. 8d and Fig. 8e.

A closer examination of the end-of-immersion changes at the IMP level for the UD24 and UD72 samples (Fig. 7b,c - EoI) shows that the inhibiting layers are generally similar in size and activity (orange to yellow-orange in the colour scale). The same degree of activity is observed for the sites in the replicate tests (Fig. 8a-c). Notably, the UD72 sample in Fig. 7 has two high-activity sites extending beyond the usual IMP boundary (white arrows in Fig. 7c EoI map) and with much higher activity (yellow in the colour scale). These sites indicate extensive precipitation and corrosion product deposition from local corrosion of the underlying particle. However, this is uncommon, as most sites in the UD72 sample show less extensive activity. The low occurrence of such high-activity sites in UD72, despite an immersion duration three times longer than UD24, suggests that inhibiting layer growth is slow even at prolonged exposure.

Although UD24 and UD72 apparently have comparable degrees of local Ce precipitation at the end of re-immersion, their subsequent local activity during re-immersion are considerably different. During re-immersion of the UD24 sample, signs of IMP activation within the first 600 s of exposure to the inhibitor-free electrolyte similar to the UD03 sample were observed. The activity includes a low/high (see yellow arrow in Fig. 7b - 600 s) and several high/high (see dashed white arrows in Fig. 7b - 600 s) behaviour. Despite their early onset, the increase in activity level of these sites and the activation of their surrounding matrix were slower than their UD03 counterparts. After 3600 s of re-immersion, more sites with ring-like activity (i.e., rings with low-activity centres) consistent with high/high behaviour were observed on the surface of the UD24 sample (see dashed white arrows in Fig. 7b - 3600 s). Absence of nearby activity suggests that these sites fall under the H/H-A category. As with the other UD24 active sites during re-immersion, their activity level increase and activity spread to surrounding areas were gradual and not as extensive as the L/H IMPs in UD03. Low/high behaviour is also seen at several sites at 3600 s of re-immersion (see yellow arrows in Fig. 7b - 3600 s). These sites had low activity during immersion but are near areas showings signs of Ce(III) deposition. The corrosion of these sites is triggered by the inhibiting layer failure on the adjacent areas between 600 and 3600 s (Movie 3). This makes the sites candidates for L/H-B behaviour. Substantial dealloying and trenching is observed around these sites leading to development of high activity (see yellow arrows in Fig. 7b - 7200 s). The activation of these L/H sites shows that even with 24 h of immersion in the inhibited solution, some particles can still present with minimal interaction with the inhibitor which makes them prone to corrosion

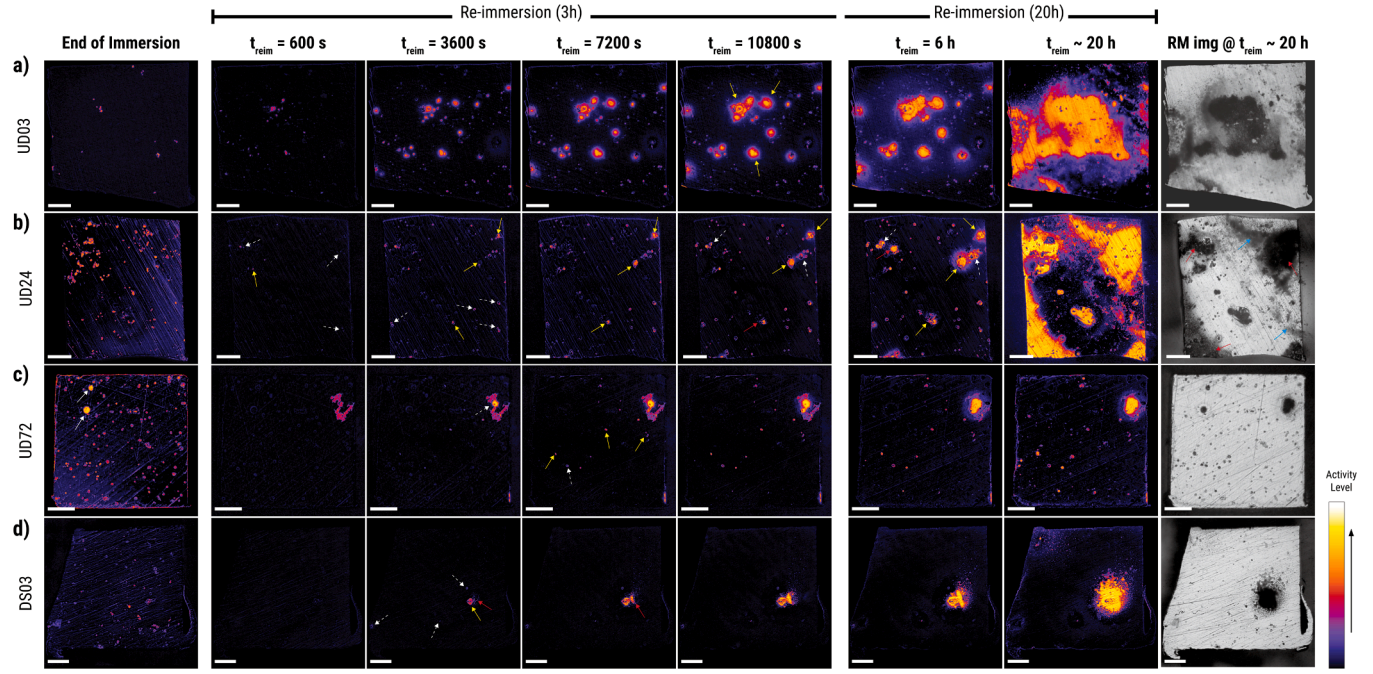

Fig. 7. Global activity maps of AA2024 samples immersed in 0.05 M NaCl + 0.001 M Ce(III) under different conditions: (a) 3 h, (b) 24 h, (c) 72 h, and (d) with a 30-second inhibitor supply delay, immersed for 3 h. The first column shows the sample state at the end of the initial immersion. The second to fifth columns display changes during re-immersion in 0.05 M NaCl for 3 h, while the last three columns show changes during extended re-immersion. White scale bars represent 100 μm.

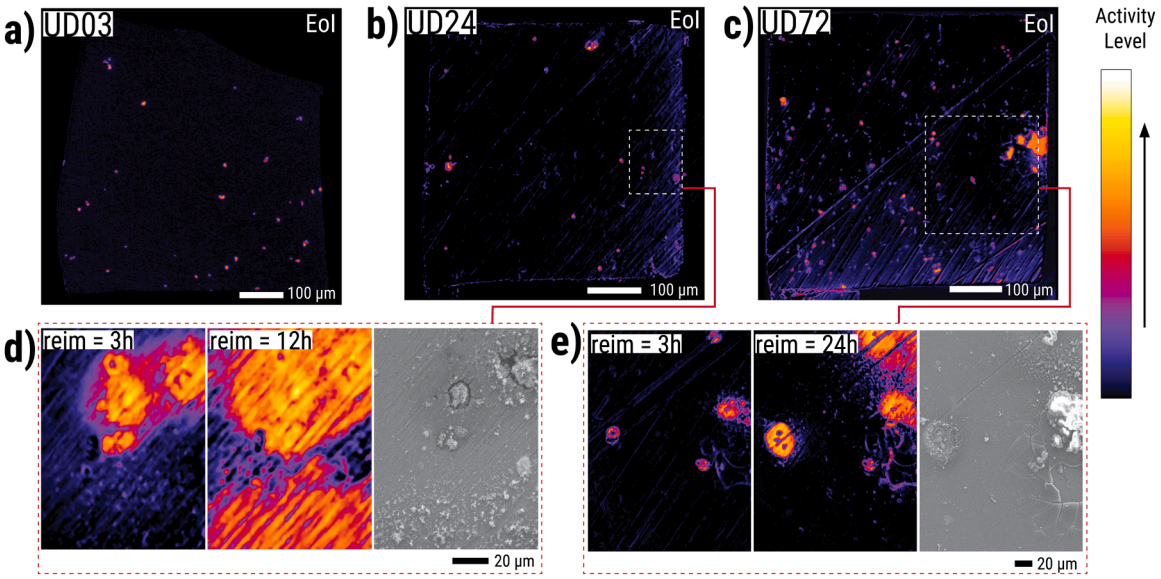

Fig. 8. Activity maps at the end of immersion (EoI) for replicate samples exposed to 0.05 M NaCl with 0.001 M $Ce(NO_3)_3$ for (a) 3 h, (b) 24 h, and (c) 72 h. Ce(III) was present from the start of the immersion. Panels (d) and (e) show activity maps and corresponding secondary electron (SE) images after re-immersion of the 24-hour (UD24) and 72-hour (UD72) samples, respectively. The UD24 sample was re-immersed for 12 h and the UD72 sample for 24 h before the SE images were taken.

during re-immersion. At 10800 s of re-immersion, the L/H site on the upper right corner of the sample (see yellow arrows in Fig. 7b - 10800 s) appear to be inducing activation of nearby particles based on the visible increase in active area from 7200 s. Meanwhile, the L/H site near the centre of the sample appear to trigger what appears to be intergranular corrosion (see red arrow in Fig. 7b - 10800 s). Fig. 9 provides a close up the activity progression of this site. On the other hand, the H/H sites maintain gradual activity level increase and activity spread to the surrounding areas. This is evident when the corrosion around clusters of active sites with H/H behaviour (see dashed white arrows in Fig. 7b - 10800 s) is compared with that of active site clusters from UD03. H/H active site clusters in UD24 had limited activity spread while active site clusters in UD03 exhibited considerable development of high activity on a large portion of the matrix around the IMPs (see yellow arrows in Fig. 7a - 10800 s). This indicates that although the thick inhibiting layers fail, they can still slow down local corrosion progression likely by limiting redistribution of Cu particles from the IMP surface. This slow progression is further observed in the status of the H/H cluster after 6 h of re-immersion (see dashed white arrow in Fig. 7b – 6 h). However, their relative stability is undermined by the propagating activity coming

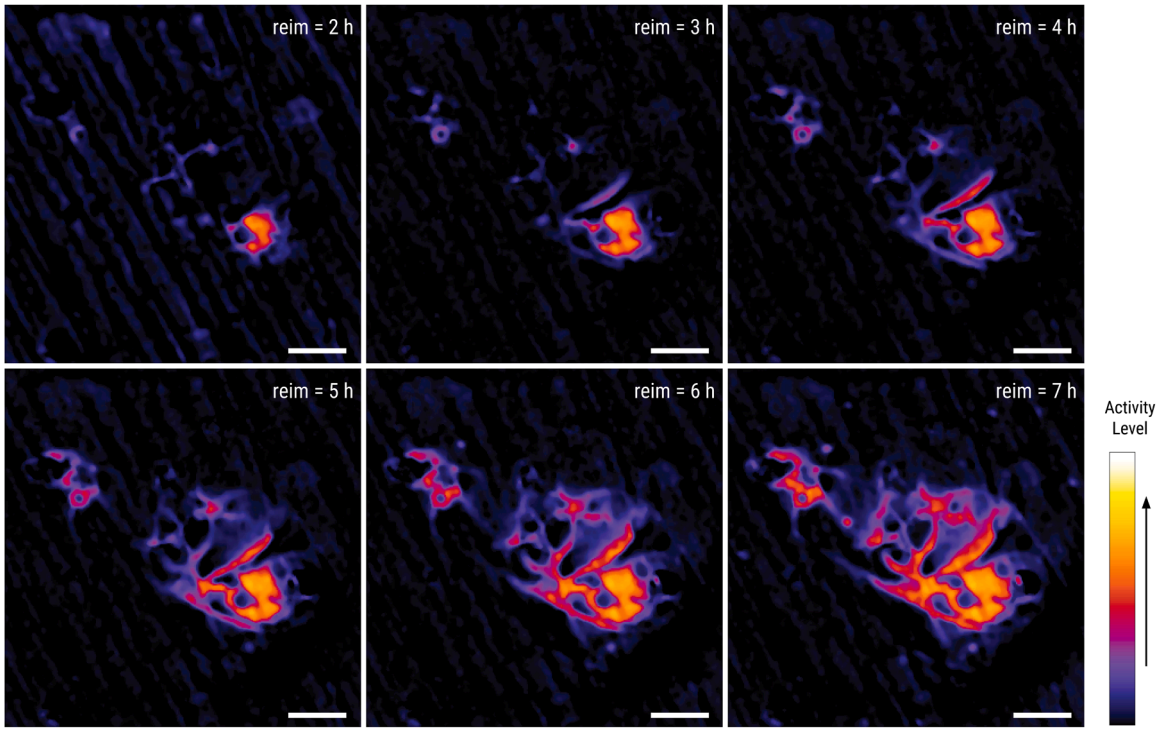

Fig. 9. Activity progression on the suspected intergranular corrosion site in Fig. 7b. The local corrosion is characterized by gradual growth of activity along filaments instead of the typical radial spread from an intermetallic particle.

from the L/H sites (see yellow arrows in Fig. 7b – 6 h). A new L/H site near the upper left corner (see red arrow in Fig. 7b – 6 h) also developed somewhere between 3 and 6 h of re-immersion. Extended re-immersion to 20 h does show inhibition failure leading to significant matrix involvement (i.e., large areas of yellow-level activity) comparable to that of UD03. Corresponding raw reflected light microscopy images that these areas have extensive matrix dissolution (see red arrows in Fig. 7b – RM image at 20 h) and are covered by corrosion product deposits (see cyan arrows in Fig. 7b – RM image at 20 h). Majority of the matrix dissolution and corrosion product generation can be traced to cooperative corrosion from the areas with L/H sites (Movie 3). L/H sites in the UD24 replicate also drove local corrosion development during re-immersion (Supporting Information 5).

Majority of the IMPs in the UD72 sample exhibited low activity (dark purple-coloured sites) during the first 600 s of re-immersion. A rapid matrix dissolution event was observed on the upper right corner of the sample surface (Movie 4). The visual appearance of the dissolution event is comparable to streaking corrosion reported in AA7075-T6 [50,51] which suggests that it is some form of a surface layer attack [52,53]. It is noted though that this event was only observed in this test and thus requires further validation. Nonetheless, the dissolution event appear to have affected IMPs in that region and induced their inhibition failure. This resulted to the appearance of a highly active site (yellow-coloured site) in the area at around 1 h of re-immersion (see dashed arrow in Fig. 7c - 3600 s). Gradual spread of activity from this site to surrounding matrix is observed for the rest of the re-immersion. Initiation of inhibition loss in other sites also became visible at around 2 h of re-immersion. These inhibition loss sites include several with low/high (see yellow arrows in Fig. 7c - 7200 s) and one with high/high (see dashed white arrow in Fig. 7c - 7200 s) behaviour. The activity increase and activity spread to the adjacent matrix of these sites were gradual based on their limited size increase at three hours of re-immersion (Fig. 7c - 10800 s). Additionally, at three hours of re-immersion, the number of the active sites in UD72 is less than those in UD03 or UD24. Kosari et al. [14] reported that at prolonged exposure to the Ce (III)-containing environment, gradual dealloying of IMPs eventually leaves a Cu-rich remnant. This remnant can facilitate cathodic reactions with sufficient oxygen supply and subsequently lead to substantial local changes. Absence of such changes suggests that the inhibiting layer in UD72 is less permeable than those formed in UD24 or UD03. Stability of these inhibiting layers lead to low matrix involvement even at 20 h of re-immersion (Fig. 7c – 20 h). Local re-immersion activity in the UD72 replicate is also limited to a few H/H sites (Fig. 8d) and areas near the edge of the sample (Supporting Information 5).

Similar to prolonged/sustained inhibitor supply, fast inhibitor release in active corrosion protection systems is expected to minimize local corrosion. This justifies existing approach for inhibitor testing focused on immediate exposure to the inhibiting solution. Such exposure protocol is particularly relevant for AA2024 which contains IMPs that dealloy within the first minute of exposure to NaCl [37]. Sufficient mitigation of local corrosion is still possible when the inhibitor is not immediately available to the surface. This was shown in our previous work on delayed inhibitor supply for AA2024 wherein inhibitor supply delay of less than or equal to one minute led to surface changes less extensive than uninhibited systems [28]. Delayed inhibitor supply approximates slower inhibitor release rates from coatings which in itself is a viable strategy to extend inhibitor availability (and prolong exposure time). Fig. 7d shows global activity maps for AA2024 exposed to Ce(III) with delayed supply (DS03). Specifically, the introduction of Ce(III) was delayed by 30 s to allow limited IMP dealloying progression. Movie 5 shows a time-lapse of the surface changes during the re-immersion of DS03 in 0.05 M NaCl. The DS03 EoI activity map (Fig. 7d – End of Immersion) shows that when Ce(III) is delayed, more active sites observed at the end of the 3 h immersion time compared to UD03 (Fig. 7a – End of Immersion). The activity levels of the sites range from purple to orange in the activity colour scale.

Supplementary material related to this article can be found online at doi:10.1016/j.corsci.2025.113146.

During re-immersion, visible loss of inhibition is not observed until around 3600 s when several high/high (dashed white arrows in Fig. 7d – 3600 s) and low/high (yellow arrow in Fig. 7d – 3600 s) sites are seen around the centre and left edge of the sample. The high/high sites exhibited minimal activity level increase and spread. Meanwhile, the low/high site, which appears to be a composite IMP based on the connected IMP outlines seen on the EoI in Fig. 7d, exhibited visible changes on the IMP surfaces consistent with dealloying. The activity eventually spread to the adjacent matrix (Fig. 7d – 7200 s) consistent with trenching. The activation also affected a right section of the composite IMP (red arrow in Fig. 7d – 3600 s) which showed low level activity during immersion. The dealloying and trenching of this IMP led to more matrix dissolution and considerable corrosion product deposition with further re-immersion (red arrow at Fig. 7d – 7200 s).

The midALs of active sites measured from different immersion conditions – UD03, UD24, UD72, and DS03 – were used for quantitative comparison of stability during re-immersion (Fig. 10). Active sites are sites that exhibited activity levels above the threshold of 20 either at the end of immersion or at 3 h of re-immersion. We focused on these sites instead of sampling all IMPs on the surface because they directly indicate local corrosion as discussed in Section 3.2. During immersion, they show Ce(III) precipitation triggered by dealloying. During re-immersion, they point to areas with dealloying, trenching, and possible corrosion product buildup, all of which signal a loss of inhibition. Additionally, we used the midAL of active sites at the 10800 s of re-immersion rather than overall surface changes because it directly shows loss of inhibition. In contrast, surface-wide metrics can exaggerate the impact of a few active sites especially when their cooperative corrosion leads to significant corrosion product deposition. Fig. 10 shows that midAL distribution for UD24 (median midAL = 5) and UD72 (median midAL = 1) have significantly lower median compared to UD03 (median midAL = 55.5). This is attributed to the increased frequency of active sites displaying H/L behaviour which was also seen in the activity maps during the first three hours of re-immersion. Meanwhile, The decreasing trend of mean midAL values (UD03 = 72.0, UD24 = 37.8, UD72 = 6.9) with immersion duration proves that longer exposure to the corrosion inhibitor not only improves inhibition stability when the inhibitor is present but also when the inhibitor is not available anymore. The trend is attributed to the reduction in frequency of inhibition loss events during re-immersion

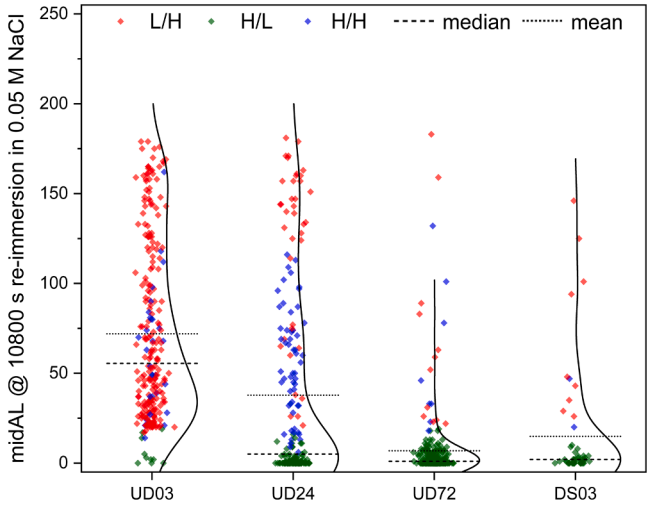

Fig. 10. Comparison of midAL after 3 h of re-immersion for active sites identified during initial immersion under different conditions: varying durations (UD03, UD24, UD72) and a 30-second inhibitor supply delay (DS03). Active sites are those where midAL exceeded 20 during either immersion or re-immersion.

(i.e., L/H and H/H active sites). Meanwhile, comparison of the median midAL of UD03 and DS03 (median midAL = 2) shows higher H/L frequency with delayed supply (green points). The mean midAL of the DS03 active sites (mean = 14.9) also indicates less extensive inhibition loss events during re-immersion compared to UD03 despite their similar immersion durations. This suggest that delayed inhibitor supply is more beneficial for re-immersion stability compared to immediate availability of the inhibitor in the corrosive media. As shown in our previous work [28], delayed inhibitor supply allows limited dealloying of the IMP surface which increases its capacity to precipitate Ce. Apart from the increase in Ce precipitation capacity, the initial exposure to the corrosive environment also allows removal of passive layers which prevent IMPs from interacting sufficiently with the inhibitor during immersion. While these passive layers offer some degree of protection, their breakdown during re-immersion can lead to exposure of the underlying IMP and uncontrolled local corrosion. The findings related to delayed inhibitor supply offer insight potentially applicable in the design of active corrosion protection systems. Since delayed inhibitor supply approximates slow release, the results also suggest that fine-tuning the initial release rates may be a more efficient strategy for long-term active corrosion protection than simply increasing inhibitor storage capacity of corrosion protection systems. It is also noted that the release rate is more controllable than the exposure times to the inhibiting solution, which is highly-dependent on environmental conditions.

4. Conclusion

The loss of inhibition at the level of individual IMPs in AA2024 during re-immersion in an inhibitor-free electrolyte shows significant variability. In general, their behaviour can be grouped based on whether they show low or high activity during the initial immersion (with inhibitor) and during re-immersion (without inhibitor). This behaviour results from a complex interplay of factors, including IMP composition, spatial distribution, and the extent of Ce(III) precipitation on their surfaces. Because these factors interact in a complex manner, the resulting immersion/re-immersion activity patterns (e.g., low/low, low/high, high/low, high/high) appear stochastic, making reliable prediction difficult. This highlights the importance of studying a large number of IMPs to capture the range of possible local corrosion behaviours. Using this analysis approach on our system (i.e., 3 h immersion in 0.05 M NaCl + 0.001 M $Ce(NO_3)_3$ followed by re-immersion in 0.05 M NaCl) revealed that the inhibiting layer formed during immersion influenced how the surface changes during re-immersion. It also introduced site-specific behaviour that would likely be missed by a global or a highly local means of analysis. The analysis also showed that most active sites during re-immersion have low activity during immersion (i.e., low degree of cerium precipitation). As such, increasing Ce(III) precipitation on the IMP surface appears to be a viable strategy for improving re-immersion stability.

Evaluation of the impact of immersion duration on re-immersion stability showed that longer exposure (e.g., up to 72 h) is indeed beneficial for minimizing loss of inhibition. Similarly, comparison of re-immersion stability for delayed (i.e., 30 s delay) and undelayed inhibitor supply for the same immersion duration (i.e. 3 h) revealed that a slight delay also enhances re-immersion performance. In both cases, the improvement is attributed to increased Ce(III) precipitation. It is noted though that these findings are specific to Ce(III)-NaCl system. Further studies are needed to assess whether similar improvements occur with other inhibitor and electrolyte combinations as well as different concentration levels. Overall, the results underscore the potential advantages of designing active corrosion protection systems that promote stronger inhibitor interaction, within limits that do not compromise system performance, to achieve better re-immersion stability.

CRediT authorship contribution statement

Santiago J. Garcia: Writing – review & editing, Writing – original draft, Supervision, Methodology, Funding acquisition, Formal analysis, Conceptualization. **Arjan Mol:** Writing – review & editing, Writing – original draft, Supervision, Formal analysis, Conceptualization. **Marlon Mopon:** Writing – review & editing, Writing – original draft, Visualization, Methodology, Investigation, Formal analysis.

Declaration of Competing Interest

The authors declare the following financial interests/personal relationships which may be considered as potential competing interests: co-author is one of the current Editors-in-Chief of Corrosion Science - A. M. If there are other authors, they declare that they have no known competing financial interests or personal relationships that could have appeared to influence the work reported in this paper.

Acknowledgements

The author acknowledges the financial support by the DOST ERDT Program and the Faculty of Aerospace Engineering at TU Delft.

Appendix A. Supporting information

Supplementary data associated with this article can be found in the online version at doi:10.1016/j.corsci.2025.113146.

Data availability

Data can be accessed in the 4TU.ResearchData online repository via this link: https://doi.org/10.4121/240a1c9a-f21f-4998-8880-5dfc6da84895.

References

[1] L. Paussa, F. Andreatta, D. De Felicis, E. Bemporad, L. Fedrizzi, Investigation of AA2024-T3 surfaces modified by cerium compounds: a localized approach, Corros. Sci. 78 (2014) 215–222, https://doi.org/10.1016/J.CORSCI.2013.10.001.
[2] F.F. Chen, I. Cole, A.E. Hughes, A.M. Glenn, E. Sapper, J. Osborne, Microstructure characterisation and reconstruction of intermetallic particles, Mater. Corros. 65 (2014) 664–669, https://doi.org/10.1002/MACO.201307345.
[3] A.E. Hughes, R. Parvizi, M. Forsyth, Microstructure and corrosion of AA2024, Corros. Rev. 33 (2015) 1–30, https://doi.org/10.1515/corrrev-2014-0039.
[4] C. Li, X. Guo, G.S. Frankel, Corrosion inhibition of AA2024-T3 by a coating containing dual-pH sensitive, corrosion inhibitor loaded microspheres, Corros. Sci. 192 (2021) 109835, https://doi.org/10.1016/J.CORSCI.2021.109835.
[5] D. Snihirova, S.V. Lamaka, M.M. Cardoso, J.A.D. Condeço, H.E.C.S. Ferreira, M. De Fatima Montemor, pH-sensitive polymeric particles with increased inhibitor-loading capacity as smart additives for corrosion protective coatings for AA2024, Electro Acta 145 (2014) 123–131, https://doi.org/10.1016/J.ELECTACTA.2014.09.009.
[6] D. Snihirova, L. Liphardt, G. Grundmeier, F. Montemor, Electrochemical study of the corrosion inhibition ability of “smart” coatings applied on AA2024, J. Solid State Electrochem. 17 (2013) 2183–2192, https://doi.org/10.1007/S10008-013-2078-3/FIGURES/9.
[7] G. Williams, H.N. McMurray, Inhibition of filiform corrosion on organic-coated AA2024-T3 by smart-release cation and anion-exchange pigments, Electro Acta 69 (2012) 287–294, https://doi.org/10.1016/J.ELECTACTA.2012.03.002.
[8] P.J. Denissen, S.J. Garcia, Cerium-loaded algae exoskeletons for active corrosion protection of coated AA2024-T3, Corros. Sci. 128 (2017) 164–175, https://doi.org/10.1016/j.corsci.2017.09.019.
[9] R. Oltra, F. Peltier, Influence of mass transport on the competition between corrosion and passivation by inhibitor release after coating breakdown, Prog. Org. Coat. 92 (2016) 44–53, https://doi.org/10.1016/J.PORGCOAT.2015.11.024.
[10] E. Javierre, S.J. García, J.M.C. Mol, F.J. Vermolen, C. Vuik, S. Van Der Zwaag, Tailoring the release of encapsulated corrosion inhibitors from damaged coatings: controlled release kinetics by overlapping diffusion fronts, Prog. Org. Coat. 75 (2012) 20–27, https://doi.org/10.1016/J.PORGCOAT.2012.03.002.
[11] S.G.R. Emad, S. Morsch, T. Hashimoto, Y. Liu, S.R. Gibbon, S.B. Lyon, X. Zhou, Leaching from coatings pigmented with strontium aluminium polyphosphate inhibitor pigment- evidence for a cluster-percolation model, Prog. Org. Coat. 137 (2019) 105340, https://doi.org/10.1016/J.PORGCOAT.2019.105340.

[12] L. Paussa, F. Andreatta, D. De Felicis, E. Bemporad, L. Fedrizzi, Investigation of AA2024-T3 surfaces modified by cerium compounds: a localized approach, Corros. Sci. 78 (2014) 215–222, https://doi.org/10.1016/J.CORSCI.2013.10.001.
[13] J. Zhao, A. Santoso, S.J. Garcia, Small concentrations of NaCl help building stable inhibiting layers from 2,5-dimercapto-1,3,4-thiadiazole (DMTD) on AA2024-T3, Corros. Sci. 225 (2023) 111562, https://doi.org/10.1016/J.CORSCI.2023.111562.
[14] A. Kosari, M. Ahmadi, F. Tichelaar, P. Visser, Y. Gonzalez-Garcia, H. Zandbergen, H. Terryn, J.M.C. Mol, Editors' Choice—dealloying-driven cerium precipitation on intermetallic particles in aerospace aluminium alloys, J. Electrochem Soc. 168 (2021) 041505, https://doi.org/10.1149/1945-7111/abf50d.
[15] K.A. Yasakau, M.L. Zheludkevich, S.V. Lamaka, M.G.S. Ferreira, Mechanism of corrosion inhibition of AA2024 by rare-earth compounds, J. Phys. Chem. B 110 (2006) 5515–5528, https://doi.org/10.1021/JP0560664/ASSET/IMAGES/MEDIUM/JP0560664E00026.GIF.
[16] B.R.W. Hinton, Corrosion inhibition with rare earth metal salts, J. Alloy. Compd. 180 (1992) 15–25, https://doi.org/10.1016/0925-8388(92)90359-H.
[17] G. Williams, A.J. Coleman, H.N. McMurray, Inhibition of Aluminium Alloy AA2024-T3 pitting corrosion by copper complexing compounds, Electro Acta 55 (2010) 5947–5958, https://doi.org/10.1016/J.ELECTACTA.2010.05.049.
[18] P.J. Denissen, V. Shkirskiy, P. Volovitch, S.J. Garcia, Corrosion inhibition at scribed locations in coated AA2024-T3 by cerium- and DMTD-loaded natural silica microparticles under continuous immersion and wet/dry cyclic exposure, ACS Appl. Mater. Interfaces 12 (2020) 23417–23431, https://doi.org/10.1021/ACSAMI.0C03368/ASSET/IMAGES/LARGE/AM0C03368_0003.JPEG.
[19] P.J. Denissen, S.J. Garcia, Cerium-loaded algae exoskeletons for active corrosion protection of coated AA2024-T3, Corros. Sci. 128 (2017) 164–175, https://doi.org/10.1016/J.CORSCI.2017.09.019.
[20] F. Maia, J. Tedim, A.D. Lisenkov, A.N. Salak, M.L. Zheludkevich, M.G.S. Ferreira, Silica nanocontainers for active corrosion protection, Nanoscale 4 (2012) 1287–1298, https://doi.org/10.1039/C2NR11536K.
[21] S.V. Lamaka, M.L. Zheludkevich, K.A. Yasakau, M.F. Montemor, M.G.S. Ferreira, High effective organic corrosion inhibitors for 2024 aluminium alloy, Electro Acta 52 (2007) 7231–7247, https://doi.org/10.1016/J.ELECTACTA.2007.05.058.
[22] D. Snihirova, S.V. Lamaka, P. Taheri, J.M.C. Mol, M.F. Montemor, Comparison of the synergistic effects of inhibitor mixtures tailored for enhanced corrosion protection of bare and coated AA2024-T3, Surf. Coat. Technol. 303 (2016) 342–351, https://doi.org/10.1016/J.SURFCOAT.2015.10.075.
[23] T.G. Harvey, S.G. Hardin, A.E. Hughes, T.H. Muster, P.A. White, T.A. Markley, P. A. Corrigan, J. Mardel, S.J. Garcia, J.M.C. Mol, A.M. Glenn, The effect of inhibitor structure on the corrosion of AA2024 and AA7075, Corros. Sci. 53 (2011) 2184–2190, https://doi.org/10.1016/j.corsci.2011.02.040.
[24] C. Özkan, L. Sahlmann, C. Feiler, M. Zheludkevich, S. Lamaka, P. Sewlikar, A. Kooijman, P. Taheri, A. Mol, Laying the experimental foundation for corrosion inhibitor discovery through machine learning, npj Mater. Degrad. 2024 8 1 (8) (2024) 1–15, https://doi.org/10.1038/s41529-024-00435-z.
[25] A.M. Homborg, M. Olgiati, P.J. Denissen, S.J. Garcia, An integral non-intrusive electrochemical and in-situ optical technique for the study of the effectiveness of corrosion inhibition, Electro Acta 403 (2022) 139619, https://doi.org/10.1016/J.ELECTACTA.2021.139619.
[26] P. Visser, H. Terryn, J.M.C. Mol, On the importance of irreversibility of corrosion inhibitors for active coating protection of AA2024-T3, Corros. Sci. 140 (2018) 272–285, https://doi.org/10.1016/J.CORSCI.2018.05.037.
[27] Z. Li, A. Homborg, Y. Gonzalez-Garcia, A. Kosari, P. Visser, A. Mol, Evaluation of the formation and protectiveness of a lithium-based conversion layer using electrochemical noise, Electro Acta 426 (2022) 140733, https://doi.org/10.1016/J.ELECTACTA.2022.140733.
[28] M. Mopon, A. Mol, S.J. Garcia, Effect of delayed inhibitor supply on AA2024-T3 intermetallic activity: a local in situ analysis with reflected microscopy, Corros. Sci. 230 (2024) 111910, https://doi.org/10.1016/J.CORSCI.2024.111910.
[29] R. Parvizi, A.E. Hughes, M. Forsyth, M.Y. Tan, Probing localised corrosion inhibition of AA2024-T3 by integrating electrode array, SVET, SECM, and SEM-EDS techniques, Metals 2023 13 (2023) 1703, https://doi.org/10.3390/MET13101703.
[30] Z. Lai, D. Li, S. Cai, M. Liu, F. Huang, G. Zhang, X. Wu, Y. Jin, Small-area techniques for micro- and nanoelectrochemical characterization: a review, Anal. Chem. 95 (2023) 357–373, https://doi.org/10.1021/ACS.ANALCHEM.2C04551/ASSET/IMAGES/LARGE/AC2C04551_0007.JPEG.
[31] W. Chang, H. Qian, Z. Li, A. Mol, D. Zhang, Application and prospect of localized electrochemical techniques for microbiologically influenced corrosion: a review, Corros. Sci. 236 (2024) 112246, https://doi.org/10.1016/J.CORSCI.2024.112246.
[32] N. Jadhav, V.J. Gelling, Review—the use of localized electrochemical techniques for corrosion studies, J. Electrochem Soc. 166 (2019) C3461–C3476, https://doi.org/10.1149/2.0541911JES/XML.
[33] L.B. Coelho, M. Taryba, M. Alves, X. Noirfalise, M.F. Montemor, M.G. Olivier, The corrosion inhibition mechanisms of Ce(III) ions and triethanolamine on graphite—AA2024-T3 galvanic couples revealed by localised electrochemical techniques, Corros. Sci. 150 (2019) 207–217, https://doi.org/10.1016/J.CORSCI.2019.02.007.
[34] T. Hu, H. Shi, D. Hou, T. Wei, S. Fan, F. Liu, E.H. Han, A localized approach to study corrosion inhibition of intermetallic phases of AA 2024-T3 by cerium malate, Appl. Surf. Sci. 467468 (2019) 1011–1032, https://doi.org/10.1016/J.APSUSC.2018.10.243.
[35] M. Olgiati, P.J. Denissen, S.J. Garcia, When all intermetallics dealloy in AA2024-T3: quantifying early stage intermetallic corrosion kinetics under immersion, Corros. Sci. (2021) 109836, https://doi.org/10.1016/j.corsci.2021.109836.
[36] A.M. Homborg, M. Olgiati, P.J. Denissen, S.J. Garcia, An integral non-intrusive electrochemical and in-situ optical technique for the study of the effectiveness of corrosion inhibition, Electro Acta 403 (2022) 139619, https://doi.org/10.1016/J.ELECTACTA.2021.139619.
[37] M. Olgiati, P.J. Denissen, S.J. Garcia, When all intermetallics dealloy in AA2024-T3: quantifying early stage intermetallic corrosion kinetics under immersion, Corros. Sci. (2021) 109836, https://doi.org/10.1016/j.corsci.2021.109836.
[38] C.A. Schneider, W.S. Rasband, K.W. Eliceiri, NIH Image to ImageJ: 25 years of image analysis, Nat. Methods 9 (7) (2012) 671–675, https://doi.org/10.1038/nmeth.2089.
[39] J. Li, N. Birbilis, R.G. Buchheit, Electrochemical assessment of interfacial characteristics of intermetallic phases present in aluminium alloy 2024-T3, Corros. Sci. 101 (2015) 155–164, https://doi.org/10.1016/J.CORSCI.2015.09.012.
[40] L. Lacroix, L. Ressier, C. Blanc, G. Mankowski, Combination of AFM, SKPFM, and SIMS to study the corrosion behavior of S-phase particles in AA2024-T351, J. Electrochem Soc. 155 (2008) C131, https://doi.org/10.1149/1.2833315/XML.
[41] L. Lacroix, C. Blanc, L. Ressier, Localized corrosion mechanisms of 2024 aluminum alloy: atomic force microscopy and kelvin force microscopy contribution, ECS Meet. Abstr. MA2009-02 (2009) 1735, https://doi.org/10.1149/MA2009-02/16/1735.
[42] K.H. Gayer, L.C. Thompson, O.T. Zajicek, The solubility of aluminum hydroxide in acidic and basic media at 25 °C, Https://Doi.Org/10.1139/V58-184 36 (2011) 1268–1271, https://doi.org/10.1139/V58-184.
[43] A. Kosari, F. Tichelaar, P. Visser, H. Zandbergen, H. Terryn, J.M.C. Mol, Dealloying-driven local corrosion by intermetallic constituent particles and dispersoids in aerospace aluminium alloys, Corros. Sci. 177 (2020) 108947, https://doi.org/10.1016/j.corsci.2020.108947.
[44] A. Kosari, H. Zandbergen, F. Tichelaar, P. Visser, P. Taheri, H. Terryn, J.M.C. Mol, In-situ nanoscopic observations of dealloying-driven local corrosion from surface initiation to in-depth propagation, Corros. Sci. 177 (2020), https://doi.org/10.1016/J.CORSCI.2020.108912.
[45] X. Zhou, C. Luo, T. Hashimoto, A.E. Hughes, G.E. Thompson, Study of localized corrosion in AA2024 aluminium alloy using electron tomography, Corros. Sci. 58 (2012) 299–306, https://doi.org/10.1016/J.CORSCI.2012.02.001.
[46] A.E. Hughes, T.A. Markley, S.J. Garcia, J.M.C. Mol, Comparative study of protection of AA 2024-T3 exposed to rare earth salts solutions, Corros. Eng. Sci. Technol. 49 (2014) 674–687, https://doi.org/10.1179/1743278214Y.0000000172.
[47] T. Hu, H. Shi, T. Wei, F. Liu, S. Fan, E.H. Han, Cerium tartrate as a corrosion inhibitor for AA 2024-T3, Corros. Sci. 95 (2015) 152–161, https://doi.org/10.1016/J.CORSCI.2015.03.010.
[48] S.J. Garcia, T.A. Markley, J.M.C. Mol, A.E. Hughes, Unravelling the corrosion inhibition mechanisms of bi-functional inhibitors by EIS and SEM–EDS, Corros. Sci. 69 (2013) 346–358, https://doi.org/10.1016/J.CORSCI.2012.12.018.
[49] A.E. Hughes, A.M. Glenn, N. Wilson, A. Moffatt, A.J. Morton, R.G. Buchheit, A consistent description of intermetallic particle composition: an analysis of ten batches of AA2024-T3, Surf. Interface Anal. 45 (2013) 1558–1563, https://doi.org/10.1002/SIA.5207.
[50] R.S. Huang, C.J. Lin, H.S. Isaacs, Measuring streaking rates of an Al–Zn alloy using a difference imaging technique, Corros. Sci. 48 (2006) 1867–1873, https://doi.org/10.1016/J.CORSCI.2006.05.039.
[51] R.S. Huang, C.J. Lin, H.S. Isaacs, A difference-imaging technique used to study streaking corrosion of aluminum alloys AA7075 and AA8006 in chloride solution, Electrochem. SolidState Lett. 9 (2006) B11, https://doi.org/10.1149/1.2140503/XML.
[52] Z. Zhao, G.S. Frankel, On the first breakdown in AA7075-T6, Corros. Sci. 49 (2007) 3064–3088, https://doi.org/10.1016/J.CORSCI.2007.02.001.
[53] S.-S. Wang, F. Yang, G.S. Frankel, Effect of altered surface layer on localized corrosion of aluminum alloy 2024, J. Electrochem Soc. 164 (2017) C317–C323, https://doi.org/10.1149/2.1541706JES/XML.